Polydisperse Granular Packings and Bearings

Von der Fakultät Mathematik und Physik der Universität Stuttgart
zur Erlangung der Würde eines Doktors der
Naturwissenschaften (Dr. rer. nat.) genehmigte Abhandlung

vorgelegt von

Reza Mahmoodi Baram
Shiraz, Iran

Hauptberichter:	Prof. Dr. Hans J. Herrmann
Mitberichter:	Prof. Dr. Hans-Rainer Trebin
Tag der mündlichen Prüfung:	Juli 22, 2005

Institut für Computeranwendungen 1 der Universität Stuttgart

2005

The Kiss Precise

For pairs of lips to kiss maybe
Involves no trigonometry.
'T is not so when for circles kiss
Each one the other three.
To bring this off the four must be:
As three in one or one in three.
If one in three, beyond a doubt
Each gets three kisses from without.
If three in one, then is that one
Thrice kissed internally.

Four circles to the kissing come.
The smaller are the benter.
The bend is just the inverse of
The distance form the center.
Though their intrigue left Euclid dumb
There's now no need for rule of thumb.
Since zero's bend's a dead straight line
And concave bends have minus sign,
The sum of the squares of all four bends
Is half the square of their sum.

To spy out spherical affairs
An oscular surveyor
Might find the task laborious,
And now besides the pair of pairs
A fifth spere in the kissing shares.
Yet, signs and zero as before,
For each to kiss the other four
The quare of the sum of all five bends
Is thrice the sum of their squares.
Frederick Soddy
Soddy, F., Nature **137** *1021, 1936.*

Publications related to this thesis

- R. Mahmoodi Baram and H.J. Herrmann. *Self-Similar Space-Filling Packings in Three Dimensions*. Fractals, **12**, 293-301 (2004).
- R. Mahmoodi Baram, H.J. Herrmann, and N. Rivier. *Space-Filling Bearings in Three Dimensions*. Phys. Rev. Lett., **92**, 044301-1 (2004).
- R. Mahmoodi Baram, H.J. Herrmann. *Random Bearings and Their Stability*. For submitting to Phys. Rev. Lett.
- H.J. Herrmann, J.A. Åström, and R. Mahmoodi Baram *Rotations in Shear Bands and Polydisperse Packings*. Proceedings for Angra dos Reis, Physica A, **344**, 516-522 (2004).
- H.J. Herrmann, R. Mahmoodi Baram, and M. Wackenhut *Searching for The Perfect Packing*. Proceedings for Eilat conference, Physica A, **330**, 77-82 (2003).
- H.J. Herrmann, R. Mahmoodi Baram, and M. Wackenhut *Polydisperse Packings*. Brazilian Journal of Physics, **33**, 591 (2003).
- R. Mahmoodi Baram, M. Wackenhut, and H.J. Herrmann, *The art of packing densely*. Proceedings of the International Conference on Statistical Physics of Complex Fluids, Zanjan, Iran, to be published in J. of Phys. CM

Contents

Chapter 1

Zusammenfassung

Dichte, Größenverteilung der Teilchen, sowie die Topologie und Kontaktnetzwerke gehören zu den wichtigsten Eigenschaften granularer Materialen [1]. Zur Herstellung von Hochleistungszementen werden Mischungen aus Teilchen unterschiedlicher Größe benötigt, um höhere Dichten zu erzeugen. Die raumfüllenden Lager, die wir in Kapitel 4 beschreiben, sind alle Beispiele für Systeme mit einer Dichte von 1, d.h. jede Konfiguration beschreibt eine Größenverteilung kugelförmiger Teilchen mit denen das Volumen auf mindestens eine Weise vollständig gefüllt werden kann. Hierdurch entfällt jegliche obere theoretische Grenze für die Größenverteilung.

Für die Herstellung selbstähnlicher raumfüllender Packungen in zwei und drei Dimensionen haben wir einen Algorithmus auf Basis konformer Packungen entwickelt. Mit diesem Algorithmus und einigen Erweiterungen wurden verschiedene bisher unbekannte Kugelpackungen erzeugt. Diese Packungen haben unterschiedliche Topologien, da sie verschiedene fraktale Dimensionen aufweisen. Durch definierte Einfärbung bestimmter Teilchen werden die Unterschiede der Packungen noch offensichtlicher.

Unter den dreidimensionalen Packungen gibt es eine, bei der man die einzelnen Teilchen mit nur zwei Farben so markieren kann, daß sich niemals zwei Kugeln mit der selben Farbe berühren (siehe Abb. 1.1). Wir nennen solche Konfigurationen bichromatisch. Die Bichromatik ist eine grundlegende Eigenschaft, da sie es ermöglicht, ein dreidimensionales, volumenfüllendes Kugellager zu bauen in dem die Kugeln rotieren können, ohne daß sie blockieren. Wir haben die Exis-

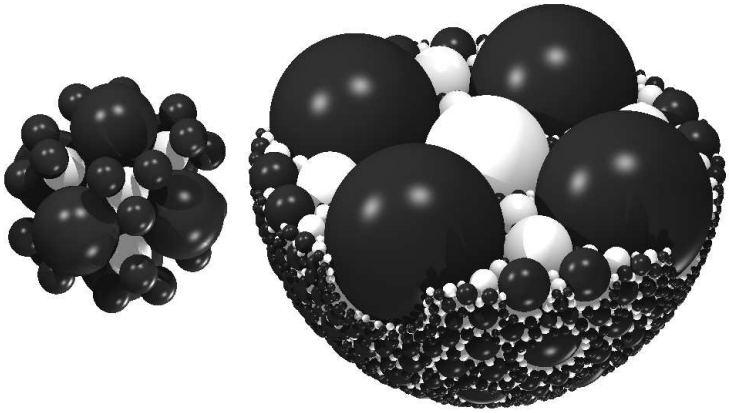

Figure 1.1: Darstellung der bichromatischen Packung, der als zweiter Packung der Oktaeder zu Grunde liegt. Kugeln der gleichen Farbe berühren sich hier nicht.

tenz des dreidimensionalen volumenfüllenden Kugellagers durch die Darstellung der genauen Konstruktion bewiesen. Wir zeigen, daß in zwei und in drei Dimensionen die Bichromatik der Packung eine notwendige und hinreichende Bedingung ist. Außerdem geben wir eine Ausdruck für die Winkelgeschwindigkeit (5.12) jeder Kugel in der Packung, die nur von ω_1 und einem Faktor c abhängen. Somit können wir das Modell, dass das Gleiten tektonischer Platten durch Rollen einzelner Teilchen beschreibt, untermauern. Dieses Ergebnis ist auch für die Mechanik und Hydrodynamik von Interesse.

Des Weiteren beschreiben wir eine Möglichkeit, zufällige Kugelpackungen zu erzeugen für ein realistischeres Modell zur Beschreibung der physikalischen Phänomene, wie sie zwischen tektonischen Platten vorkommen. Jedwede Abweichung von der perfekten Packung verursacht lokale Blockaden, die wiederum zur Energiedissipation führen. Wir zeigen, daß die Anzahl dieser Blockaden abnimmt, je größer die Anzahl der Teilchen in so einer zufälligen Packung ist. Hierdurch wird das System im Ganzen stabiler.

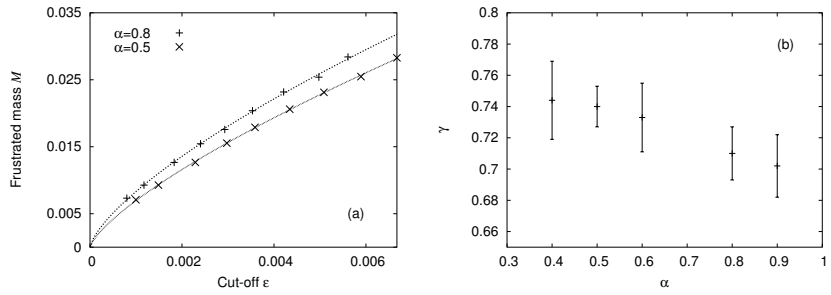

Figure 1.2: (a) Blockierte Masse $\mathcal{M}$ als Funktion des Cutoff ε für zweidimensionale Kugellager mit $\alpha = 0.5$ bzw. 0.8. Die Linien zeigen verschiedene Fits an Potenzgesetze, mit den jeweiligen Exponenten γ=0.74 und γ=0.71. (b) Der Exponent γ als Funktion von α.

Um den Einfluss der Schwerkraft auf das System zu bestimmen, gebrauchen wir eine halb-dynamische Simulationsmethode; eine Erweiterung derjenigen, die von Manna et al. [2] genutzt wurde, um Scheiben unter Gravitationseinfluss zu simulieren. Die Teilchen, welche nicht genügend Kontakte besitzen (d. h. mindestens zwei in zwei Dimensionen bzw. drei in drei Dimensionen), um ihr Eigengewicht zu tragen, müssen sich entweder im freien Fall befinden oder übereinander hinwegrollen. Alle Teilchen werden nacheinander von oben nach unten ausgewählt und dahingehend überprüft, ob sie durch ihre Kontakte mit anderen fixiert sind. Falls nicht, dann rollt das entsprechende Teilchen, oder es fällt, bis es mit einem weiteren zusammenstößt. Nach einer Abfolge von Roll- und Fallbewegungen wird das Teilchen an einer bestimmten Stelle im System anhalten und dort fixiert bleiben. Abb. 1.2(a) zeigt die Blockierte Masse $\mathcal{M}$ als Funktion des Cutoff ε für zweidimensionale Kugellager mit Konstruktionsparameter $\alpha = 0.5$ bzw. 0.8. Der beste Fit an die Datenpunkte wird durch eine Potenzfunktion $\mathcal{M} \sim \varepsilon^{\gamma}$ erzielt. ε ist definiert als der Cutoff der Teilechengröße. Der Exponent γ wurde für verschiedene Werte von α berechnet, wie in Abb. 1.2(b) gezeigt.

Die Ergebnisse lassen darauf schließen, dass das System sich einem Zustand völliger Stabilität annähert, d. h. $\mathcal{M} = 0$ für $\varepsilon \to 0$. Bei einem endlichen Cutoff besteht eine endliche Energie-Dissipation, welche mit kleiner werdendem Cutoff verschwindet. Der Exponent γ nimmt —innerhalb der Rechengenauigkeit— einen mehr oder weniger konstanten Wert, nämlich 0.72 ± 0.02 an. Dies deutet auf ein allgemein gültiges Verhalten der Energie-Dissipationsrate eines

zufälligen Kugellagers als Funktion des Cutoffs hin.

Diese Arbeit leistet einen wichtigen Beitrag auf diesem Feld und eröffnet die Möglchkeit für weitere Forschung. Die Untersuchung von Raumpackungen und Kugellagern ist ein junges Forschugnsgebiet und bietet ein großes Potential für weitere Arbeiten, theoretisch als auch experimentell. Im Folgenden sollen einige Möglichkeiten für weitere Arbeiten besprochen werden.

In Wirklichkeit sind die Teilchen zufällig verteilt, und es ist sehr unwahrscheinlich dass eine einzige bestimmte Konfiguration angenommen wird. Ein statistischer Zugang scheint daher unausweichlich. Es ist noch unklar, ob es eine weitere Konfiguration derselben Größenverteilung gibt, die zur gleichen Dichte führt. Dies wirft eine wichtige Frage auf: Was ist die maximale Dichte für eine vorgegebene Verteilung an Teilchen. Außer für den speziellen Fall wo alle Teilchen dieselbe Größe haben, ist diese Frage bisher noch nicht ausreichend untersucht worden.

Chapter 2

Introduction

2.1 Granular media

Substances known as *granular media* include anything that is made up of macroscopically-sized solid particles. According to material scientist Patrick Richard, "Granular materials are ubiquitous in nature and are the second-most manipulated material in industry (the first one is water)" [3]. Bulk quantities of these materials display behavior which is unlike that of either solids or liquids and studies of the granular state continue to produce surprising results that are unique to this class of matter [4–10]. Unlike solids, granular media conform to the shape of a container and will flow if the container is tilted sufficiently. Unlike liquids, however, a granular material is stable when its container is tilted slightly. In addition, they exhibit a wealth of interesting phenomena like heaping under vibration [11–14], segregation [15–17], convection [18], heap-formation [19, 20], fluidisation [21, 22], and density waves [23, 24].

A distinguishing feature between flows of granular materials and other solid-fluid mixtures is that in granular flows, the direct interaction of particles plays an important role in the flow mechanics [25]. A significant fraction of the energy dissipation and momentum transfer in granular flows occurs when particles are in contact with each other or with a boundary. Following are a few examples of granular flows:

- grains such as corn or wheat flowing from a silo

- landslides of boulders and debris
- rock and ice collisions in planetary rings
- dune formation
- transport and handling of coal or chemicals in industrial plants
- powder metallurgy
- handling of pharmaceuticals

Granular media include common materials as diverse as sand, wheat, flour, soil, coal, seeds, pills, etc. and, therefore, play an important role in many of our industries, such as mining, agriculture, civil engineering and pharmaceutical manufacturing. They clearly are also important for geological processes where landslides and erosion and, on a larger scale, plate tectonics determine much of the morphology of the Earth. However, their physics remains poorly understood (for a nice review of what is known, look into *Physics of the Granular State* by H.M. Jaeger S.R. Nagel in Science, Vol. 255, 20 March 1992, page 1523), and there is no generally accepted theory of granular media so far. Therefore, in recent years the simulation of granular systems has become a widely used research tool. The growing capacity of computer power gives rise to the hope to achieve a significant progress in the understanding of the complicated collective behavior of granular media in the near future.[1]

2.2 Contribution of the present work

Density, size distribution of the particles, topology and contacts network are among the most important properties of granular materials [1]. In high performance concrete (HPC), mixtures of particles with different sizes which lead to larger densities are highly desired. Although mixing techniques are of practical importance, the size distribution of the particles plays also a crucial role in order to get densities as large as possible, since it puts sometimes theoretical higher bound on the density [26]. For example, for a mono-disperse mixture of the spherical particles the highest possible density that can be ever reached is ≈ 0.74 which is for highly ordered configurations of face-centered cubic packing (FCC)

[1] This text was adapted from the introduction to the article *The Physics of Granular Materials* by Heinrich M. Jaeger, Sidney R. Nagel, and Robert P. Behringer which appeared in Physics Today, April 1996, page 32.

and hexagonal close packing (HCP). The space-filling bearings which we will discuss in Ch. 4 are all clear examples of systems with density one. In other words, each configuration presents a size distribution for spherical particles with which the space can be completely filled in least in one way. This removes any upper theoretical limit on the density for this particular size distribution.

The topology and the contact network are important in the dynamic behavior such as energy dissipation and shear stress in dense systems [27–29]. Shear bands and tectonic plates are examples of such systems. In both of which there is a relatively thin layer where the largest dissipation and stress release occur.

The present work is a contribution to this fast-growing field of research, by developing techniques for constructing packings and bearings which consist of ideally round particles of a variety of sizes using mainly geometric approaches. Several configurations are constructed here for the first time. The only previously-known self-similar space-filling packing in three dimensions is the classic Apollonian packing.

Furthermore, we develop a method for constructing random bearings as more realistic models for physical phenomena such as the tectonic plates. Any deviation from the perfect bearing causes the formation of frustrated arrangements of the particles in a system, resulting in dissipation of energy.

2.3 Overview

In Ch. 3, a brief introduction to the concepts and methods which we will encounter in this work is given. In Ch. 4, we develop a technique for constructing different self-similar space-filling packings in both two- and three-dimensions. In Ch. 5, we discuss general bearings in two and three dimensions for ideally round particles and show that one of the constructed packings can act as a bearing. In Ch. 6, we introduce a method for constructing more realistic bearings in which the particles are distributed randomly in space. We also study the effect of gravity on the stability of such bearings using a semi-dynamics and measure the amount of energy dissipation which may occur when the particle sizes have a lower bound. Finally, a conclusion is presented in chapter 7.

Chapter 3

Basics

3.1 Sphere packing

In mathematics, sphere packing problems are problems concerning arrangements of non-overlapping identical spheres which fill a space. Usually the space involved is three-dimensional Euclidean space. However, sphere packing problems can be generalized to two dimensional space (where the "spheres" are circles), to n-dimensional space (where the "spheres" are hyper-spheres) and to non-Euclidean spaces such as hyperbolic space.

A typical sphere packing problem is to find an arrangement in which the spheres fill as large a proportion of the space as possible. The proportion of space filled by the spheres is called the density of the arrangement. As the density of an arrangement can vary depending on the volume over which it is measured, the problem is usually to maximize the average or asymptotic density, measured over a large enough volume.

A regular arrangement (also called a periodic or lattice arrangement) is one in which the centers of the spheres form a very symmetric pattern called a lattice. Arrangements in which the spheres are not arranged in a lattice are called irregular or aperiodic or random arrangements.

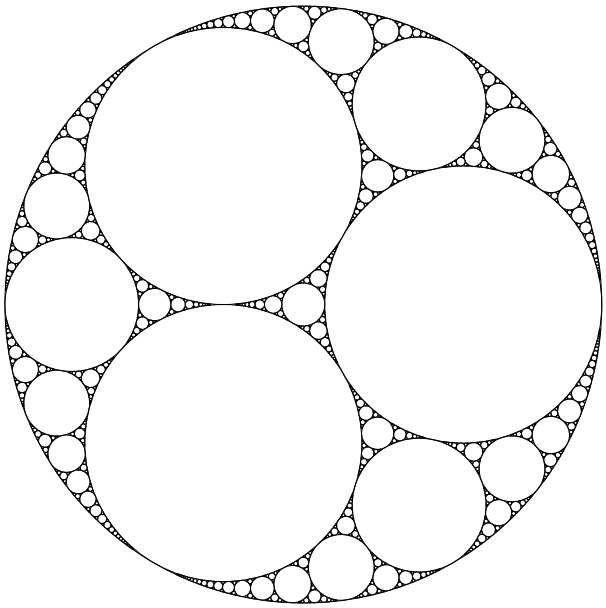

Figure 3.1: Apollonian packing of circles.

3.1.1 Circle packing

In two dimensional Euclidean space, German mathematician Carl Friedrich Gauss proved that the regular arrangement of equal-sized circles with the highest density is the hexagonal packing arrangement, in which the centers of the circles are arranged in a hexagonal lattice (like a honeycomb), and each circle is surrounded by six other circles. The density of this arrangement is

$$\frac{\pi}{\sqrt{12}} \sim 0.9069$$

In 1940, the Hungarian mathematician László Fejes Tóth proved that the hexagonal lattice is the densest of all possible circle packings, both regular and irregular.

However, in order to get higher densities, the monodispersity condition should be abandoned. Depending on the amount of particles of each size, the maximum

possible density varies over a wide range. Therefore, the size distribution of particles is a crucial property of the packing. It is possible to obtain even the density *one* by systematically choosing right sizes and positions for the particles. An example is the well known *Apollonian* packing, in which one starts with three mutually touching circles and puts in the hole between them a fourth circle which touches all three, and iterates the same procedure (see Fig. 3.1.) To find the radius of the fourth r_4 circle which touches three mutually tangent circles of radii r_1, r_2 and r_3, René Descartes has given a formula in a letter in 1643 to Princess Elisabeth of Bohemia [30]:

$$\left[\left(\frac{1}{r_1}\right)+\left(\frac{1}{r_2}\right)+\left(\frac{1}{r_3}\right)+\left(\frac{1}{r_4}\right)\right]^2 = 2\left[\left(\frac{1}{r_1}\right)^2+\left(\frac{1}{r_2}\right)^2+\left(\frac{1}{r_3}\right)^2+\left(\frac{1}{r_4}\right)^2\right] \tag{3.1}$$

This formula was rediscovered in 1936 by the physicist Sir Frederick Soddy who expressed it in the form of a poem, 'The Kiss Precise' [31]. Apollonian packing is an example of two dimensional self-similar space-filling packing.

The same configuration can be obtained in other ways. Herrmann et al. obtained a variety of classes of such configurations, among which Apollonian packing is a special case, using a technique based on conformal mappings [32, 33]. These configurations were obtained in pursuit of space filling bearings in which the particles can role on each other and no particles rub on another one. The necessary and sufficient condition for a packing to act as a bearing is that any closed loop of touching particle should contain an even number of particles. Figure 3.2 shows two examples of space-filling bearings. The upper configuration has loop size four and the lower one has loop size six. In this work, we use a technique which is in principle similar but with the difference that it can be easily extended to three-dimensions (see Ch. 4).

3.1.2 Sphere packing

In three dimensional Euclidean space, Gauss proved that the regular arrangements of equal-sized spheres with the highest density are two very similar arrangements called cubic close packing (or face centered cubic) and hexagonal

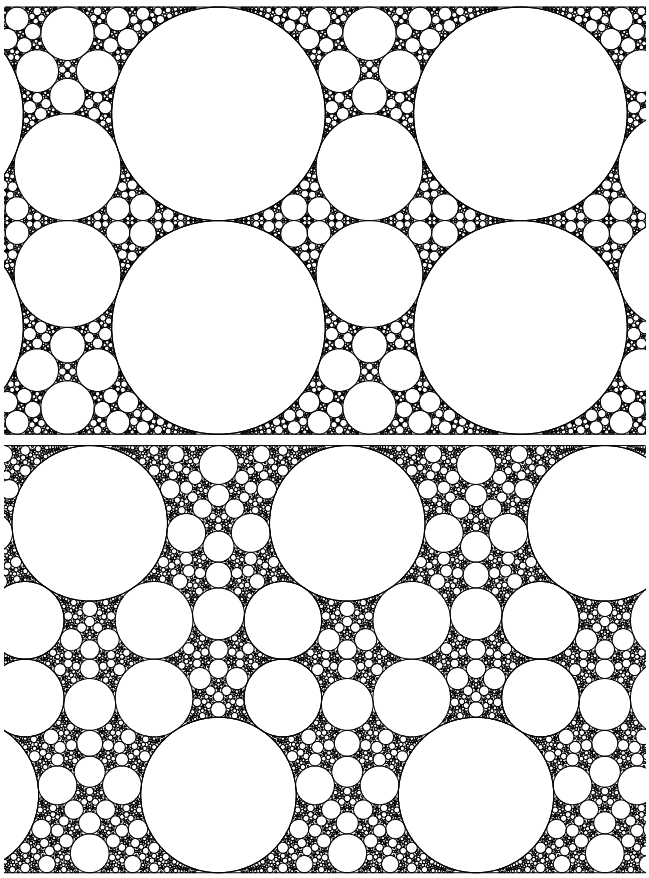

Figure 3.2: Examples of space-filling bearings in two dimensions.

close packing. In both of these arrangements each sphere is surrounded by 12 other spheres, and both arrangements have an average density of

$$\frac{\pi}{\sqrt{18}} \sim 0.7405$$

In 1661 Johannes Kepler had conjectured that this is the maximum possible density for both regular and irregular arrangements - this became known as the Kepler conjecture. In 1998 Thomas Hales, Andrew Mellon Professor at the University of Pittsburgh, announced that he had a proof of the Kepler conjecture. Hales'

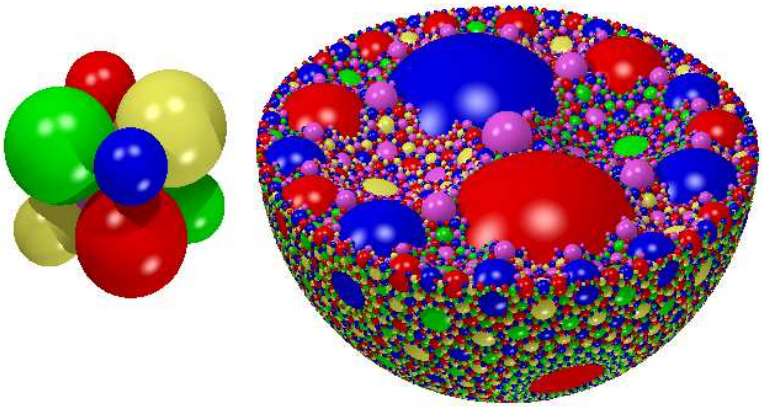

Figure 3.3: Three dimensional Apollonian packing.

proof is a proof by exhaustion involving checking of many individual cases using complex computer calculations. Referees have said that they are ”99% certain” of the correctness of Hales’ proof, so the Kepler conjecture has almost certainly been proved.

As can be seen, the maximum possible density that can be reached in three dimensions using equal-sized particles is much lower than that of two dimensions. A curious point here is that in practice the highest possible density which could be reached using mixing techniques both in laboratories and computer simulations is ≈ 0.64 which is fairly lower than its possible limit 0.7405 [30, 34, 35]. Therefore, monodispersity appears even less favorable in three dimensions as long as dense packings are desired.

The corresponding Apollonian packing in three dimensions can be constructed by iteratively filling the void between four mutually touching spheres with a fifth sphere which is touching to all four. This configuration was reproduced by Peikert et al. using an algorithm called *inversion algorithm* which is the base of our

techniques in producing further configurations. Figure 3.3 shows a view of a three dimensional Apollonian packing (see Ch. 4.)

3.2 More real packings

When it comes to modeling the physical phenomena, there are some criticisms which can be made about the packings described in the previous sections. Perfectly round particles, highly regular arrangement, and no cut-off on the size of the particles are common properties of such packings which are all drawbacks for a model which tries to mimic reality.

Using perfectly round particles in their models is a common approximation which the scientists make to reduce the complexities and the computation time of the simulations. Some major behaviors of the granular media like segregation and fluidization can be captured very well by simulations even with this approximation. But, for some other behaviors like granular ratcheting one has to go beyond this approximation [36, 37]. Throughout this work, however, we consider the particles in the system to be perfectly round geometrical objects.

Another problem is that the packings mentioned in the last sections are highly regular. Therefore, they will not be satisfactory when it comes to modeling the physical phenomena where usually a high degree of randomness exists. There are several methods, including *random Apollonian packing* (RA packing) [38] and *packing-limited growth* (PLG) [39–41], which have been developed to construct packings mimicing the random patterns formed in nature.

In PLG objects are seeded randomly in the space and in the time. The objects, then, grow according to a rule which may be specific to each object. They stop growing when a part of their boundary hits that of another object. Some physical examples of this kind of pattern formation may be found in the competition between tree crowns in dense forests [42, 43], the structure of porous media [44–46], and the generalized problem of dense packings [47].

In the RA packing, the packing process begins in a finite-size volume (or alternatively with an initial number of disks with fixed radii). New disks are added one at a time by randomly choosing a point in the packing and inserting the largest possible disk centered at that point.

As we will discuss in Ch. 6, we develop an alternative method for filling the space which is more amenable to our eventual goal, namely, the construction of

random bearings.

The third criticism is the lack of a lower bound on the size of the particles. In Ch. 6 we will study in detail the effect of an external force such as gravity on the random packings we obtain in Ch. 5, when a lower bound exists for the size of the particles.

3.3 Bearings and plate tectonics

Space-filling bearings have been introduced in several contexts, such as in explaining the so-called seismic gaps [48–50] of geological faults. The term seismic gap refers to any region along an active geological plate boundary that has not experienced a large thrust or strike-up earthquake for more than 30 years [50]. The tectonic plates usually tend to move relative to each other due to the earth's internal convection, but the large friction between the boundaries hinders a continuous sliding which would be several centimeters per year and leads to the accumulation of stress over the course of time. Beyond a critical point the accumulated stress is released resulting in big shocks and large relative motions of the plates of up to $20m$. Figure 3.4 demonstrates San Andreas fault and nearby geological structure and how different tectonic plates move relatively.

The deformation of geomaterials produces well-known spontaneous shear planes. Due to the granular structure inside the shear planes, grains can rotate. In fact, the tectonic faults are examples of shear planes which are spontaneously formed inside a deformed earth's crust. In the upper layers of the earth's crust, where the hydrostatic pressures are not too high, the network of faults has been monitored over many orders of magnitude and self-similarity has been measured by Barton and others [51] from geological maps. Active faults flow on a layer of fragments, called gauge, which over time organizes itself into a size distribution [52] given by a power law. Also rotations have been observed in this gauge zone [48, 53, 54].

Space-filling bearings have also been used as toy models for turbulence and can also be used in mechanical devices [55]. Two dimensional space-filling bearings have been shown to exist and a discrete infinity of realizations has been constructed [32, 33]. The remaining question still open is: Do they also exist in three dimensions? This question is of fundamental importance to the physical applications.

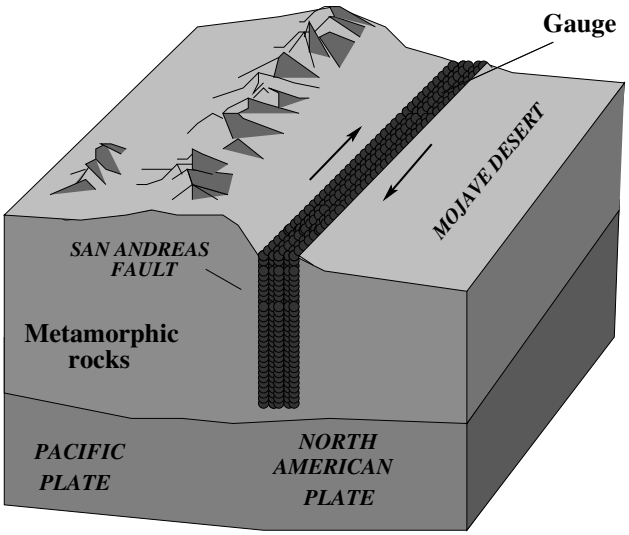

Figure 3.4: San Andreas fault and nearby geological structure. Different tectonic plates move relatively.

3.3.1 Bearing model

In some faults, like that of San Andreas, tectonic plates have been moving for a long time (thousands of years) without any significant earthquake or production of heat as it is expected for the processes involving rubbing rough surfaces. The space-filling bearings were introduced more than a decade ago for the first time by Herrmann et al. as a simplified model for explaining this phenomenon [32, 33]. In this model, it is assumed that the space between the tectonic plates is filled with more or less round particles which, as the plates move, may roll on each other resulting in the spontaneous formation of local bearings and reducing the amount of friction and dissipation of energy. One refers to the medium which fills up the gap between two plates as *gauge* (see Fig. 3.4). The spontaneous formation of bearings has been shown to be possible in simulations of shear bands [29], supporting the model.

In a tectonic fault the large blocks of rocks are, of course, not simple spheres. The most significant difference between a packing of spheres and that of closely packed irregular blocks is that the spheres can rotate on each other as in a bearing. They can also form complex ensembles of sliding grains that act like a ratchet

and effectively also perform rotations [36]. If, however, the shear stress on the blocks in the fault increases, the shape irregularities that hinder the blocks from rotating will eventually break, and blocks will begin to rotate. The introduction of fragmenting blocks has been studied in Ref. [56, 57].

In this work we extend the idea of space-filling bearing to three dimensions. Although the dynamics of bearings in three dimension is more complicated than that of two dimensions due to higher rotational degrees of freedom of the spheres, we will show in Ch. 5 that the necessary and sufficient condition for a packing of spheres to be a bearing is to be bichromatic. In other words, only two colors are needed for coloring all spheres in such a way that no spheres having the same color touch each other. One example of bearings in three dimension has been discovered among the space-filling packings which will be presented in Ch. 4.

In Ch. 6, we will improve our three dimensional model by introducing randomness in the arrangement of the particles, since such highly ordered configurations like the one among self-similar packings are very unlikely in nature.

3.3.2 Stability under gravity

As discussed before, in all packings constructed using our techniques the space is completely covered, if no lower bound is set on the size of the particles. But, in nature there is always a smallest size for the particles and, in any model describing the reality, this fact should be considered.

However, the lack of small particles, caused by setting a lower bound on the size, may result in instabilities of the arrangement of the particles. These instabilities are specially important in the bearings. Because, by changing the arrangement of the particles, an ideal bearing can be partly or even completely destroyed and can turn into a frustrated[1] configuration. We will study the stability of random bearings in Ch. 6 by simulating the effect of gravity and calculating the energy dissipation.

There are three well-known methods to simulate the full dynamics of a system of interacting particles such as a packing of spheres. They are *molecular dynamics* (MD) [58–64], *contact dynamics* (CD) [65–68], and the *event driven* method (ED) [58, 59, 68, 69]. The proper choice depends on the system and the properties

[1] Here by frustrated we mean, particles cannot roll without rubbing on each other resulting in energy dissipation in the system

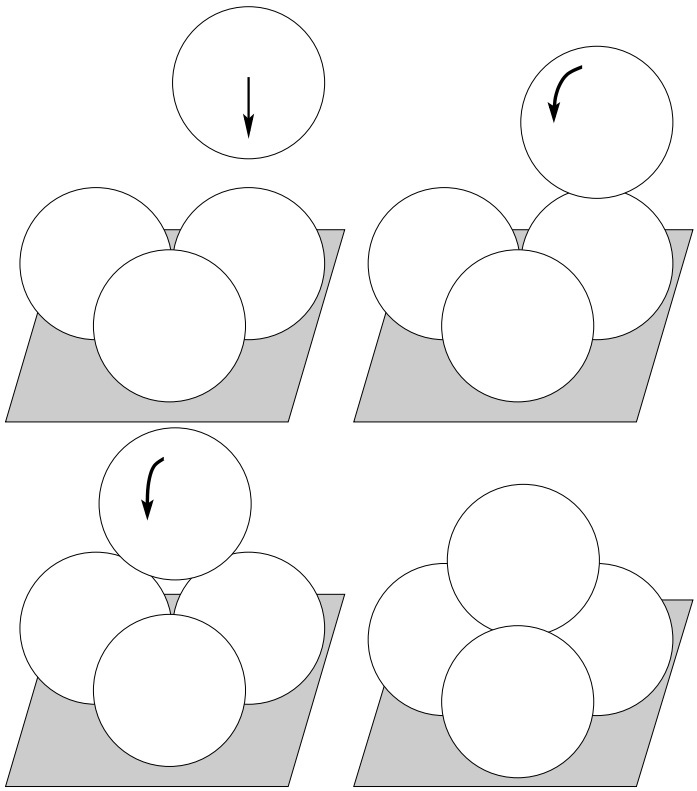

Figure 3.5: Particles fall and roll under gravity until they are fixed through their contacts with other sphere.

under consideration. While MD can be used best for dense systems, ED may be a better choice for simulating dilute systems.

To simulate the effect of gravity on our system we use a semi-dynamics in which the full details of the motion of the particles are omitted, since only the final arrangement of the particles is relevant to our problem. All particles are chosen one by one from bottom to top and checked whether they are fixed through their contacts with others. If the particle is not fixed it either rolls or falls until it hits another one. After a sequence of rollings and fallings, the particle will stop somewhere in the system and stays fixed (see Fig. 3.5.)

As discussed in Ch. 6 we can argue that the total energy dissipation will be proportional to the total mass of dislocated particles:

$$\mathcal{E}_{total} \sim \mathcal{M}.$$

Therefore, the amount of energy dissipation in the system can be calculated from the total mass of the particles which have been dislocated under gravity. Using this relation, the energy dissipation in the system which is a measure of the deviation from an ideal bearing can be studied.

3.4 Fractal dimensions

All the configurations which we will encounter throughout this work exhibit self similarity over different scales of particle sizes. In other words, the radii distribution $n(r)$ of the particles of such packings follows a power law, as we go down to smaller scales. Contrary to simple fractals, there is no known way to calculate analytically the fractal dimensions of such configurations. However, using some asymptotic functions one can calculate the fractal dimensions numerically [70–72]. The fractal dimension of a packing can be related to the exponent of its radii distribution, as follows:

$$n(r) \sim r^{-\tau}, \quad d_f = \tau - 1 \tag{3.2}$$

It can be calculated by dividing the range of the particle sizes into several intervals and counting the particles corresponding to each interval. The result can be fitted with a power-law function whose exponent is related to the fractal dimension via Eq.(3.2). However, since there will not be particles of all sizes in a packing, $n(r)$ is not a continuous function and may fluctuate strongly from one point to another. This causes difficulties in calculating the fractal dimension precisely. Some auxiliary quantities can be instead invoked for more precise calculations. These are the total number of particles $N(\varepsilon)$, the sum of the perimeters (area) of the circular (spherical) particles $s(\varepsilon)$ and the porosity $p(\varepsilon)$, i.e. the space which is not covered by particles. They are defined by introducing a cut-off length ε such that one considers in a packing exactly those circles that have a radius larger than

ε. They can be easily related to $n(r)$ as follows:

$$N(\varepsilon) = \int_{\varepsilon}^{\infty} n(r)dr \sim \varepsilon^{-d_f} \tag{3.3}$$

$$s(\varepsilon) = 2\pi \int_{\varepsilon}^{\infty} rn(r)dr \sim \varepsilon^{1-d_f} \tag{3.4}$$

$$p(\varepsilon) = 1 - \pi \int_{\varepsilon}^{\infty} r^2 n(r)dr \sim \varepsilon^{2-d_f} \tag{3.5}$$

in two dimensions and:

$$N(\varepsilon) = \int_{\varepsilon}^{\infty} n(r)dr \sim \varepsilon^{-d_f} \tag{3.6}$$

$$s(\varepsilon) = 4\pi \int_{\varepsilon}^{\infty} r^2 n(r)dr \sim \varepsilon^{2-d_f} \tag{3.7}$$

$$p(\varepsilon) = 1 - \frac{4\pi}{3} \int_{\varepsilon}^{\infty} r^3 n(r)dr \sim \varepsilon^{3-d_f} \tag{3.8}$$

in three dimensions (see Ref.[73]).

The upper limit of the integrals is actually r_{max} the size of the biggest particle in the system. However, in a finite system, for ε near r_{max} these quantities will deviate from the perfect power law and may show large fluctuations due to the effect of the walls confining the system. In the limit of $\varepsilon \to 0$ this effect vanishes and, therefore, the precise fractal dimension can be obtained considering small scales. In other words, the fractal dimension can be calculated as follows:

$$d_f = \lim_{\varepsilon \to 0} \frac{\log N(\varepsilon)}{\log \varepsilon}. \tag{3.9}$$

Similarly, d_f can be obtained from $s(\varepsilon)$ and $p(\varepsilon)$.

The fractal dimension is a topological property of a packing which can be invoked to identify the difference between the packings.

Chapter 4

Self-similar space-filling packings in three dimensions

Apart from their geometrical beauty, self-similar space-filling packings of spheres are used as models for ideally dense granular packings. For example, although we cannot expect to reproduce experimentally the precise positions of their spheres, the size distribution of such packings are good candidates to be used in making high performance concrete, if a grain of sand can be approximated as a spherical particle. The well-known Apollonian packing of circles is a two-dimensional example of such packings (see Fig. 4.1). In two dimensions, Herrmann et al [32, 33] have developed an algorithm to produce a variety of different packings of circles among which the simple Apollonian packing is a special case.

In three dimensions, only one space filling packing had been constructed and studied before (see for example Ref. [70, 74]). Peikert et al. [74] use a method called *inversion algorithm* to produce this three dimensional Apollonian packing. The inversion algorithm is based on a simple conformal transformation, namely, inversion with respect to spheres [75]. We will explain this algorithm in the following sections.

Furthermore, in this chapter, we show in detail how the inversion algorithm can be adapted to make topologically different packings of spheres which have been previously unknown. These configurations include packings with the important property of having only two classes of spheres such that no spheres from the

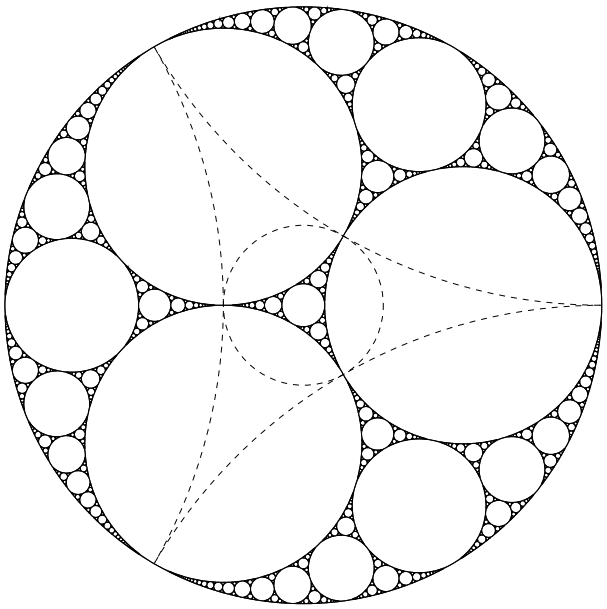

Figure 4.1: Apollonian packing of circles. The dashed circles are the inversion circles.

same class touch each other. We refer to this packings as the *bichromatic* packing which will be studied in more detail in the next chapter. We also calculate the fractal dimensions of some of new packings. As discussed briefly in the previous chapter, different fractal dimensions imply a topological difference of the packings.

In this chapter, we explain in detail the inversion algorithm and ways of its generalization in producing different packings of circles. In Sec.4.3 we go over to three dimensions and discuss all possible packings of spheres which can be obtained using our method. Finally, in Sec.4.4 we calculate the fractal dimensions of the obtained packings and of two dimensional cuts of the bichromatic packings.

4.1 Inversion algorithm

In this section we will discuss the inversion algorithm in detail.

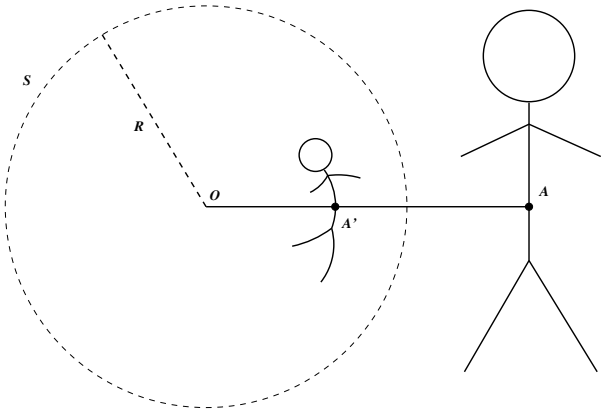

Figure 4.2: Inversion in two dimensions. Point A is mapped to point A' such that $OA \times OA' = R^2$.

4.1.1 Inversion

Following Mandelbrot [75] we refer to the inversion around a sphere S as the conformal mapping which maps any point A to another point A' along the line connecting A and center point O in such a way that:

$$OA \times OA' = R^2, \tag{4.1}$$

R being the radius of S as shown in Fig. 4.2 for two dimensions. We refer to S around which the inversion in made as *inversion sphere*. Also, A and A' are called images of each other. In an inversion around S all points outside S are mapped inside and vice versa. Only those points lying on S are mapped onto themselves. The center point O is the image of all points at infinity and any point infinitely far away is mapped to O. Applying an inversion on a point twice results in the same point.

There are two facts about the inversion as a conformal mapping which enable us to develop algorithms for construction packings:

- Angles are conserved under inversion.
- The image of a sphere is also a sphere. In other words, the set of points on a sphere are mapped under inversion into a (another) set of points on a sphere.

4.1.2 Inversion on a sphere

Throughout this chapter we will work with inversion performing on circles and spheres only. Therefore, we explore this case in detail here. Figure 4.3 illustrates how the inversion around a circle (shown as dashed) acts on different circles (shown as solid). As can be seen from the figure, there is a special case where the image of a circle falls onto itself. This is when the circle is perpendicular to the inversion circle as is the case in the lower right picture. In this case the following relation holds:

$$d^2 = R^2 + r^2, \tag{4.2}$$

where R is the radius of the inversion circle and r the radius of the circle on which the inversion is made. It can be easily verified that the same equation holds for perpendicular spheres too. One should, however, clarify the definition of the angle between two spheres. We refer to the angle between two spheres as the angle between the tangent planes at their intersection points. This angle can vary from 0 (externally tangent) to π (internally tangent) as the radii and relative distance between the centers vary. It is, of course, defined only if the two spheres intersect. For two arbitrary intersecting spheres which are not necessarily perpendicular Eq. (4.2) takes the general form:

$$d^2 = R^2 + r^2 + 2rR\cos(\alpha), \tag{4.3}$$

where α is the angle between the spheres.

As we will see in this chapter, in the construction of a packing using the inversion algorithm, both the angles between the inversion spheres and the angles between the inversion spheres and the spheres constituting the packing play crucial rules. For each packing, one needs to choose these angles properly. However, due to the geometry of the initial configuration, the possible choices which lead to a packing may be limited.

Although finding the image of a point is as easy as solving Eq. (4.1), finding the image of a sphere turns out not to be as easy. It should be noted that the center of the image of a sphere will not be in general the image of the center of that sphere, since under inversion distances are not conserved, as is shown in Fig. 4.2. In the following we calculate the image of a sphere under inversion.

A sphere can be specified by coordinates of its center and its radius (x, y, z, r). Let $S' : (x', y', z', r')$ be the image of $S : (x, y, z, r)$ under the inversion around sphere $I : (X, Y, Z, R)$. Doing some simple manipulations, one can easily derive

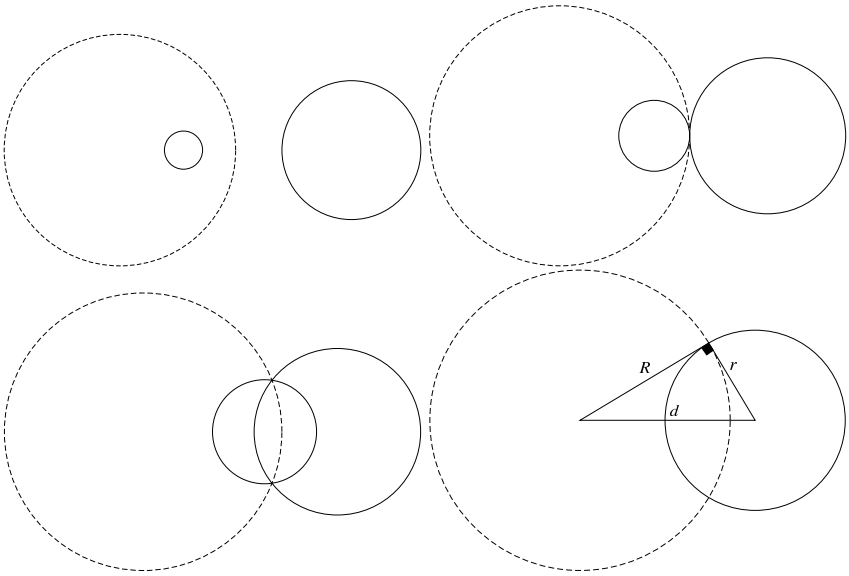

Figure 4.3: Inversion acting on different circles. The inversion circle is shown as dashed. If the circle is perpendicular to the inversion circle it is mapped onto itself.

the following relations:

$$\frac{r}{r'} = \frac{x - X}{x' - X} = \frac{y - Y}{y' - Y} = \frac{z - Z}{z' - Z} = \frac{R^2}{d'^2 - r'^2}. \tag{4.4}$$

where d' is the distance from the center of S' to the center of the inversion sphere I. This is a system of non-linear equations which cannot be easily handled especially from the computational point of view. However, one can simplify the equations using the inversion coordinates for the sphere which are defined as follows:

$$\begin{aligned} a_1 &= \frac{x}{r}, \;\; a_2 = \frac{y}{r}, \;\; a_3 = \frac{x}{r}, \\ a_4 &= \frac{x^2 + y^2 + z^2 - r^2 - 1}{2r} \\ a_5 &= \frac{x^2 + y^2 + z^2 - r^2 + 1}{2r}. \end{aligned} \tag{4.5}$$

The number of inversion coordinates is five while only four independent values

are needed in specifying a sphere. Therefore, the five coordinates are not independent and, as one can easily verify, they are related through the following equation:

$$a_1^2 + a_2^2 + a_3^2 + a_4^2 - a_5^2 = 1 \tag{4.6}$$

This choice enables us to transform the system of equations (4.4) to a linear one. The new set of equations can conveniently be written in the matrix form as follows:

$$\begin{pmatrix} a'_1 \\ a'_2 \\ a'_3 \\ a'_4 \\ a'_5 \end{pmatrix} = \tag{4.7}$$

$$\begin{pmatrix} 1-2A_1^2 & -2A_1A_2 & -2A_1A_3 & -2A_1A_4 & 2A_1A_5 \\ -2A_2A_1 & 1-2A_2^2 & -2A_2A_3 & -2A_2A_4 & 2A_2A_5 \\ -2A_3A_1 & -2A_3A_2 & 1-2A_3^2 & -2A_3A_4 & 2A_3A_5 \\ -2A_4A_1 & -2A_4A_2 & -2A_4A_3 & 1-2A_4^2 & 2A_4A_5 \\ -2A_5A_1 & -2A_5A_2 & -2A_5A_3 & -2A_5A_4 & 1+2A_5^2 \end{pmatrix} \begin{pmatrix} a_1 \\ a_2 \\ a_3 \\ a_4 \\ a_5 \end{pmatrix}$$

where $S' : (a'_1, a'_2, a'_3, a'_4, a'_5)$ is the image of $S : (a_1, a_2, a_3, a_4, a_5)$ under inversion around $I : (A_1, A_2, A_3, A_4, A_5)$. The details of the derivation of Eq. 4.8 are given in the Appendix at the end. One can simply obtain the usual coordinates of a sphere (x, y, z, r) from its inversion coordinates $(a_1, a_2, a_3, a_4, a_5)$:

$$x = ra_1, \;\; y = ra_2, \;\; z = ra_3, \;\; r = \frac{1}{a_5 - a_4}.$$

4.1.3 Iterative inversions on a sphere

Here we discuss successive inversions on a sphere performed iteratively around two spheres, since this is the main process which we utilize to construct a packing of spheres. If the inversions are made around two disjoint spheres infinitely many times, two disjoint infinite sets of images are obtained each of which confined within an inversion sphere. Figure 4.4 demonstrates an example of iterative inversions of a circle shown as solid around two inversion circles shown as dashed. The inversion spheres act similar to two parallel mirrors which produce infinite images of an object located between them, with the difference that the images becomes smaller if the inversion spheres have finite sizes.

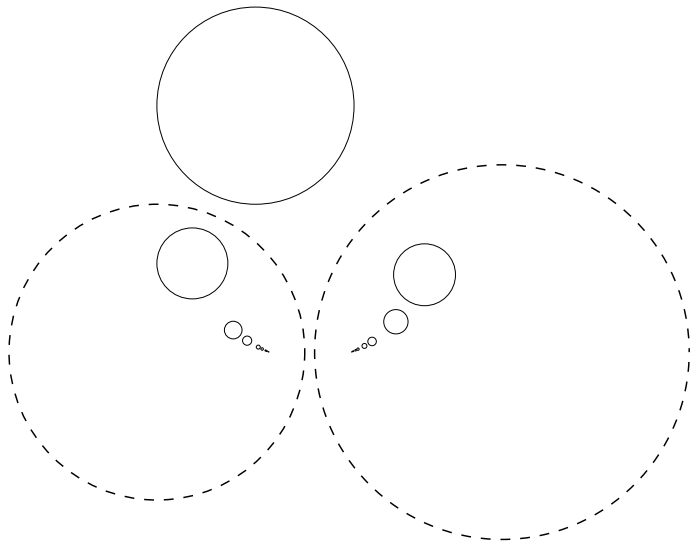

Figure 4.4: Iterative inversions applied on a circle shown as solid around two disjoint inversion circles shown as dashed.

The situation where the inversion spheres are not disjoint looks, however, different. There is an overlapping region any point of which corresponds to two points outside the inversion spheres. The left image in figure 4.5 demonstrates iterative inversions of a circle around two overlapping inversion circles. Only those inversions have been performed which decrease the size of the circles. In other words, the circles are inverted from outside of the inversions circles to inside.

It can be seen from Fig. 4.5 that the two images of original circles which fall into the overlapping region by different sequences of inversions do not necessarily fit on top of each other. This will be a problem in constructing a packing using the inversion algorithm which is based on successive inversions around inversion spheres which are overlapping. Fig. 4.11 illustrates a typical obtained configuration where the inversion circles overlap. Apparently, this is not a packing.

To resolve this problem, we take a closer look at what happens in a sequence of alternating inversions of an arbitrary circle with respect to two overlapping inversion circles. To do that, we transform the whole configuration by an inversion to a configuration which is much easier to analyze.

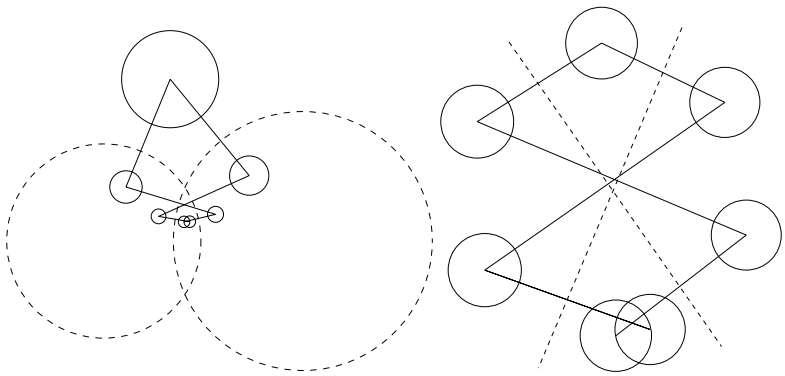

Figure 4.5: Iterative inversions of a circle with respect to two overlapping inversion circles (dashed lines). Two figures are equivalent (see the text). The solid lines connect each circle to its image.

By an inversion with respect to a circle centered around one of the intersecting points of inversion circles, the inversion circles are transformed to lines acting like plane mirrors. This is shown in Fig. 4.5 on the right. The inversion circles are now straight lines shown as dashed. The two configurations are topological equivalent, since the inversion is an conformal transformation. One can show that two circles which are images of each other will be also images of each other if the whole configuration is transformed by an inversion. To be more mathematically precise, suppose sphere S_2 is the image of S_1 under the inversion around sphere I_1, that is:

$$S_2 = \mathcal{I}_{I_1} S_1 \tag{4.8}$$

where $\mathcal{I}_{I_1}$ denotes the inversion around sphere I_1. Now, consider the inversion around sphere I_2 which is applied on S_1, S_2 and I_1, i.e.,

$$\begin{aligned} S_1' &= \mathcal{I}_{I_2} S_1 \\ S_2' &= \mathcal{I}_{I_2} S_2 \\ I_1' &= \mathcal{I}_{I_2} I_1 \end{aligned}$$

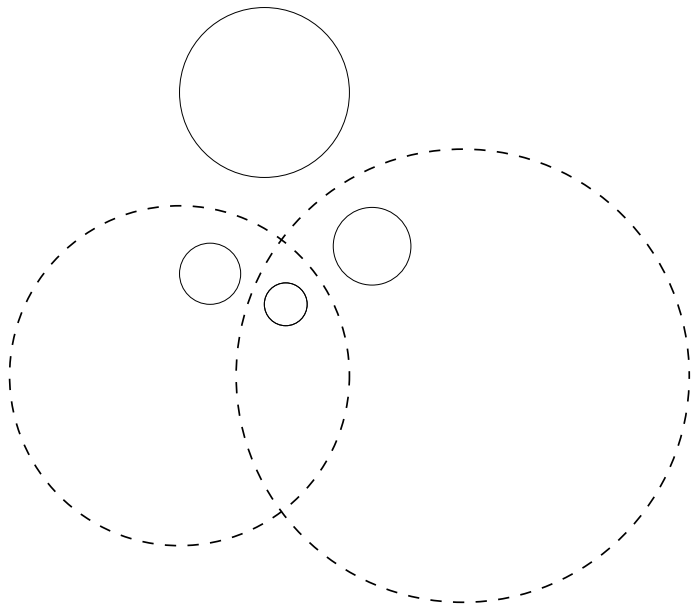

Figure 4.6: Iterative inversions on a circle shown as solid around two overlapping inversion circles shown as dashed. If the angle between the two inversion circles is chosen according to Eq. (4.11), the obtained images in the overlapping region fall exactly on top of each other (compare to Fig. 4.5).

It can be shown that:

$$S_2' = \mathcal{I}_{I_1'} S_1', \tag{4.9}$$

in other words,

$$\mathcal{I}_{I_1'} = \mathcal{I}_{I_2} \mathcal{I}_{I_1} \mathcal{I}_{I_2}^{-1} \tag{4.10}$$

Therefore, the two configurations shown in Fig. 4.5 are equivalent, as far as the inversion is concerned.

It can be seen from the figure that one can solve the problem of the overlapping of the images by choosing the angle between two inversion spheres α as follows:

$$\alpha = \frac{\pi}{l+2}, \quad l = 0, 1, 2, 3 \cdots, \tag{4.11}$$

for which the two images fall exactly on top of each other. Upon these choices the space will be divided in $2(l+2)$ regions which are images of each other with

a one-to-one correspondence between their points. As we will see in the rest of this chapter, this is why all configurations we obtain exhibit self-similarity. Figure 4.6 shows the case of $l = 0$. In Fig. 4.12 Eq. (4.11) has been considered in choosing the inversion circles.

In the following section, we will show how one can construct different space-filling bearings employing the properties of the inversion around a sphere which were discussed here.

4.1.4 Inversion as a tool for constructing packings

Self-similar space-filling packings in two dimensions were first constructed by Herrmann et al. more than one decade ago. Their technique consists of successive translations, reflections and inversions. All obtained configurations are initialized by placing two circles as seeds at very specific locations in the space between two parallel lines and applying different transformations on them in such a way that the space becomes completely filled in the limit of infinite iterations. The topology of each configuration depends on the locations of seed circles which are controlled by two integer parameters $m, n \geq 0$. The discreteness of m and n reflects the fact that the seeds cannot be chosen arbitrarily and only very special choices will result in a space-filling packing. Figure 4.7 shows some of these configuration for different values of m and n. A further condition is also implemented in their method which guarantees the number of circles in any loop to be an even number allowing for the bearing behavior. The interested readers are referred to Ref. [32] for the details on the construction of the, so-called, self-similar space-filling bearings.

In this work, we take an alternative approach different from that mentioned above. This is what we call inversion algorithm. However, the essence of our approach is the same as that of discussed above. In the following, we discuss first the traditional way of constructing the Apollonian packing. In next section, we show how the same configuration can be obtained using the inversion algorithm.

4.1.5 Apollonian packing

The Apollonian packing was discovered first by Apollonius of Perga who lived around 200BC. It can be constructed by iteratively filling the void between any

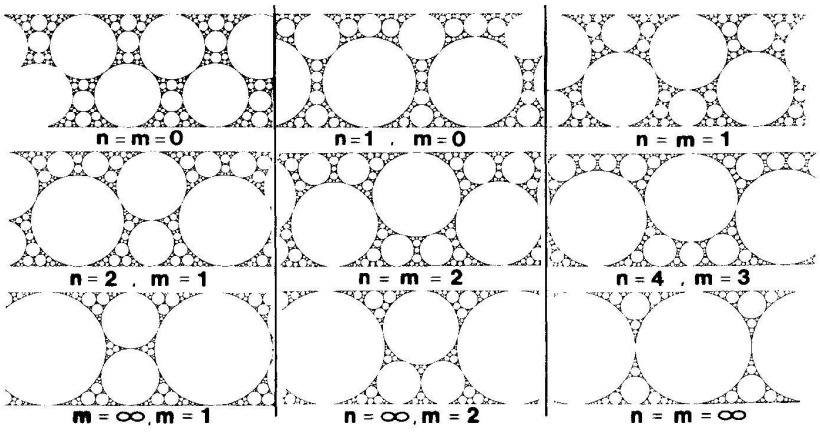

Figure 4.7: Nine different combinations of n and m of the first family.

three mutually touching circles with the biggest possible circle (see Sec. 3.1.1). The Apollonian packing is shown in Fig. 4.1.

The Apollonian packing can be alternatively constructed using the algorithm which we will explain now. This will also inspire us in generalizing the algorithm to produce new packings in two and three dimensions.

4.2 Packings in two dimensions

4.2.1 Apollonian packing using the inversion algorithm

Figure 4.8 illustrates how the inversion algorithm can be employed to construct the classic Apollonian packing of circles within an enveloping circle of unity radius. Initially three mutually touching circles are inscribed inside a circular space which is to be filled, as is shown in the upper left image. Four inversion circles (shown as dashed) are set such that each of them is perpendicular to three of the four circles (three initial circles and the enveloping unit circle.)

Beginning with this configuration, if all points *outside* an inversion circle are mapped inside, one new circle is generated, since the image of a circle perpendicular to the inversion circle falls on itself, as discussed before. If the same is

done for all the inversion circles, four new circles are generated inside the corresponding inversion circle, shown in Fig. 4.8 upper right image. We call this the first *generation*. For next generations we simply continue by applying the inversions to the newly generated circles. As mentioned before, the inversion is made only from the outside to the inside of the inversion circles. In other words, only those inversions are applied which produce a smaller circle, otherwise the circles of previous generations will be generated again. Figure 4.8 shows the initial configuration together with the three first generations. In the limit of infinite generations we obtain the well-known Apollonian packing, in which the circular space is completely filled with circles of many sizes.

Any sphere (here circle) in the packing is the result of a sequence of successive inversions on one of the initial spheres. Therefore, any sphere in the packing can be denoted by a sequence like:

$$\mathcal{I}_i\mathcal{I}_j\mathcal{I}_k\mathcal{I}_l\cdots \qquad i,j,k,l,\cdots\in\{1,2,\cdots,N_{inv}\}\,, \tag{4.12}$$

or simply $(i,j,k,l,\cdots)$, where $\mathcal{I}_i$ denotes the inversion around inversion sphere number i, and N_{inv} is the number of inversion spheres. We define the *packing coordinates* of a sphere as the sequence of positive integer numbers $(i,j,k,l,\cdots)$ which the indices of the sequential inversions take. Therefore, a typical packing coordinate is $(3,1,2,1,4)$ which represents a sphere which is obtained after five iterations. In other words, a sphere obtained after the ith iteration is represented by i indices. It should be noted that no successive indices can take a same number, since the second inversion will cancel the previous one which results the original sphere. For example, $(1,2,2,1)$ is not allowed while $(1,2,1,2)$ is allowed.

In constructing all packings two conditions are to be fulfilled:

- All free spaces should be covered, either by initial or by inversion circles
- The inversion circles can intersect with circles constituting the packing through right angles.

One can verify that these conditions are fulfilled in the construction of the Apollonian packing.

As we discussed in Sec. 4.1.3, in the case where the inversion circles overlap, a further condition should be fulfilled, namely, the angle between the inversion circles should be chosen according to Eq. (4.11). Therefore, we add a third condition:

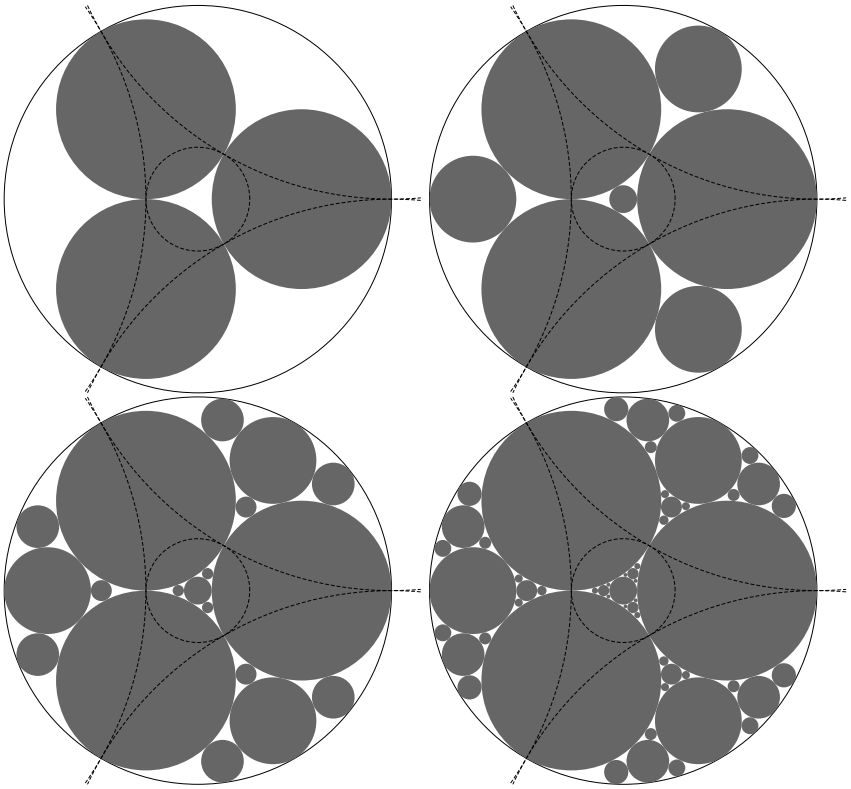

Figure 4.8: Construction of an Apollonian packing using the inversion algorithm. Inversion circles are shown as dashed.

- If the inversion spheres overlap, the angle between the inversion circles should be chosen according to Eq. (4.11).

One should be aware that the spheres generated in the overlapping regions correspond to more than one sequence of inversions. In other words, they can be represented by more than one system of coordinates, depending on the number of the inversion spheres which share that overlapping region. This means that there will be more than one copy of all the spheres generated in the overlapping regions. Furthermore, the repeated spheres are not limited to the overlapping regions, but they will spread throughout the whole packing if further inversions are applied. This is due to the self-similarity of the configuration of the packing.

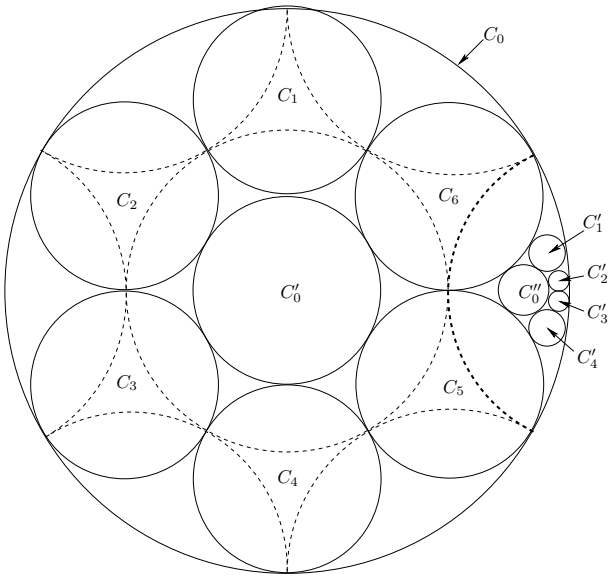

Figure 4.9: Initial circles on the six vortices of a hexagon.

Therefore, if the goal is to enumerate the spheres constituting the packing, one has to eliminate the extra copies of the spheres to obtain the correct result. This can be done simply by truncating all the sequences of inversions which generate a same sphere in the overlapping region except one. This is crucial for calculating the correct fractal dimension of the packings which is based on counting all the spheres larger than certain sizes (see Sec. 3.4).

4.2.2 Extension of the inversion algorithm

The inversion algorithm in two dimensions can be generalized in two ways, which we shall discuss here. Looking at Fig. 4.8, one realizes that the initial configuration for constructing the Apollonian packing consists of three touching circles on the vortices of an equilateral triangle inside a circular space. Three inversion circles are placed each of which corresponding to one side of the triangle perpendicular to the enveloping circle and the circles making that side. Another inversion circle is set in the center perpendicular to all three initial circles.

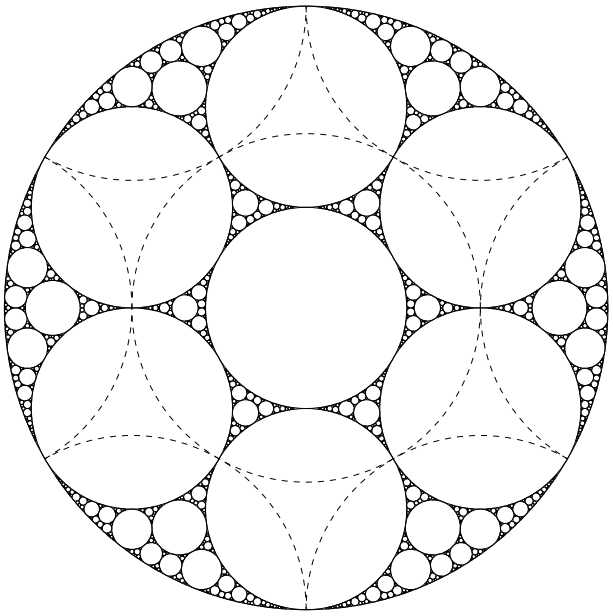

Figure 4.10: The packing based on a hexagon.

This is, however, not the only possible configuration which fulfills our initialization conditions discussed in last section. An immediate idea for finding new configurations is to set the initial circles on the vortices of a regular polygon of N sides (vortices) inside the circular space instead of a triangle. Then, $N+1$ inversion circles are to be set; N inversion circles perpendicular to the enveloping unit circle and to each pair of the initial circles which share the same side of the polygon and one inversion circle in the center perpendicular to all initial circles. It can be verified that the initialization conditions hold for any $N \geq 3$.

Figure 4.9 shows the initial configuration for $N = 6$. The circles obtained from inversions around one of the inversion circles are also shown for clarity. The final packing is represented in Fig. 4.10. This generalization will inspire us also in generalizing the three dimensional inversion algorithm.

In all mentioned initial configurations, the initial circles which make a side of the based polygon have been set to be touching each other. This is not necessary, however, and by relaxing this restriction a variety new and interesting packings

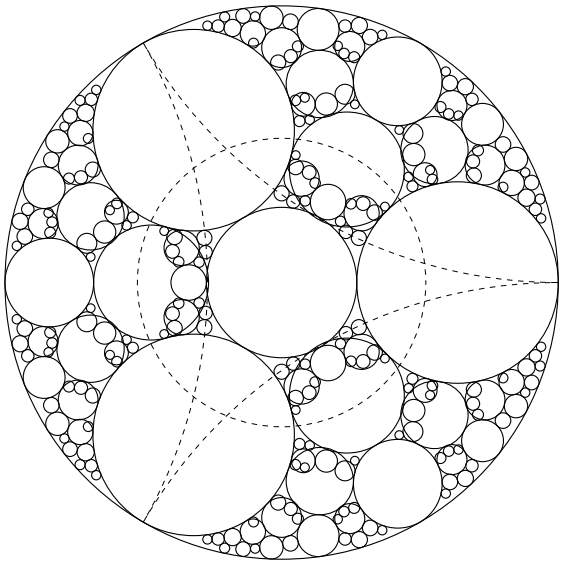

Figure 4.11: The generalization of the simple Apollonian packing to non-touching initial circles. If the angle between the inner and the outer inversion circles is *not* chosen according to Eq. (4.11) no physical packing is obtained.

can be obtained. We do this simply by reducing the sizes of the initial circles[1]. The outer inversion circles are the same as before, since in this way the touching points of initial circles with the unit circle do not change. But, the inner inversion circle should be larger in order to still be perpendicular to the initial circles, and also cover the space which is not covered by others. Apparently this causes the overlapping of the inner inversion circle with outer ones. One should, therefore, take care of the third condition of the initialization.

Considering Eq. (4.11) in choosing the size of the initial circles, we obtain an infinite number of different packings corresponding to the different values of $l \geq 0$ and $N \geq 3$. The packing with $l = 0$ and $N = 3$ is shown in Fig. 4.12. Figure 4.11 shows a case where the initial configuration has not been chosen properly.

It seems worth to mention that the classic Apollonian packing of circles shown

[1]They will be still touching the border of the circular space, since otherwise the condition of having no initially unoccupied space outside all the inversion circles is not fulfilled

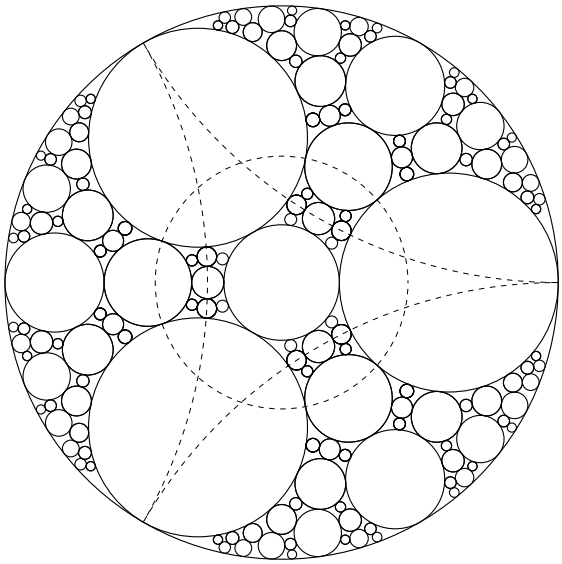

Figure 4.12: The generalization of the simple Apollonian packing to non-touching initial circles. If the angle between the inner and the outer inversion circles is chosen according to Eq. (4.11) a packing without overlapping is obtained. This packing corresponds to $l = 0$.

in Fig. 4.1 corresponds to $l = \infty$ and $N = 3$. In that case, the angle between inversion circles α is zero, that is, they are externally touching.

It may become already clear to the reader that finding new packings is a matter of finding new allowed initial configurations. In fact this is what we will do throughout the rest of this chapter. Later we will mention few techniques with which further two dimensional packings can be obtained. But, now we shall discuss the construction of three dimensional packings which is in principle the same as for their two dimensional analoga. The only difference is that the choices for the initialization of the packings are much more limited.

4.3 Generalization to three dimensions

As was mentioned before, Peikert et al. used the inversion algorithm to very efficiently make the so-called three dimensional Apollonian packing of spheres within an enveloping sphere of radius one. In this section, we use this algorithm and its generalization discussed in the previous section to produce more such three dimensional self-similar space-filling packings.

Peikert et al. begin with four initial spheres on the vortices of a tetrahedron inside a unit sphere which is to be filled. They placed five inversion spheres, four spheres perpendicular to the enveloping unit sphere and to the three initial spheres corresponding to each face of the tetrahedron, and one inversion sphere in the center perpendicular to all four initial spheres. However, the inversion spheres, even in this case which is the simplest three dimensional configuration, do overlap. We come back to this later in this section.

The fact that in two dimensions we can replace a triangle by other regular polygons as the basis for new configurations of initial circles suggests to do a similar extension in three dimensions. So, we examine the configurations based on the other *Platonic Solids* besides the tetrahedron as possible candidates. In this section, we will study all Platonic Solids and their resulting packings. An important restriction is, however, that the number of Platonic Solids is limited to five. Furthermore, as we will see in the following, the inversion spheres overlap in all configurations. Therefore we do not expect as many packings as in two dimensions. Because, decreasing the size of the initial spheres which was our trick for finding new configurations will cause further overlapping of inversion spheres, which cannot go beyond a certain extent. Actually, we will end up with only five packings.

We begin with mutually touching initial spheres on the vortices of a Platonic Solid inside the unit sphere. Inversion spheres are placed as follows; One in the center of the unit sphere perpendicular to all initial spheres, and one at each face of the Platonic Solid perpendicular to the enveloping unit sphere and the initial spheres which form that face of the Platonic Solid. Therefore, the number of vortices of the Platonic Solid determines the number of the initial spheres and the number of its faces determines the number of the inversion spheres. There will be one more inversion sphere in the center (which is perpendicular to all the initial spheres on the vortices.) The enveloping unit sphere is also considered as belonging to the initial spheres, since its images will be part of the packing. Using this configuration of initial and inversion spheres, the process of filling the space is exactly the same as explained in the last section, that is, iteratively

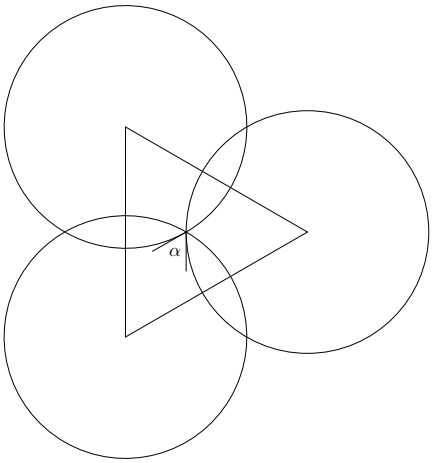

Figure 4.13: Overlapping of the inversion spheres in the case of the tetrahedron. α equals $\frac{\pi}{3}$.

mapping the initial spheres into smaller and smaller unoccupied spaces.

The spheres are grouped into different classes (assigned by different colors) such that no spheres having the same color touch each other. We consider the color coding as an another topological characteristic of a packing beside its fractal dimension. Selecting colors for the spheres needs to be done only for initial spheres. If the color of a sphere is also assigned to the images of that sphere, the same pattern will exist in the whole packing and on all scales due to the self-similarity of the configuration. In other words, for any color the neighbouring colors are always the same.

In the following we will discuss in detail each of the Platonic Solids and their possible packings.

4.3.1 Packing based on the tetrahedron

As we discussed in the last section, in order that the iterative inversions lead to an allowed packing, the inversion spheres should either not overlap or, if they do, the angle α between them should follow Eq. (4.11). As mentioned before, in three dimensions α is the angle between the planes tangent to two inversion

spheres at their intersection points. Therefore, we check the value of α for each Platonic Solid as well as, here, for the tetrahdron. To do this, we note that the centers of the inversion spheres are on the vortices of the *conjugate Platonic Solid*. Figure 4.13 shows the plane containing one of the faces of the Platonic Solid conjugate to the tetrahedron (which is also a tetrahedron). This plane is tangent to the unit sphere and to one of the initial spheres at their contact point. The circles are the cross section of the plane with the inversion spheres. One can easily see that the angle between two neigbouring inversion spheres is $\frac{\pi}{3}$, which happens to be equal to the value corresponding to $l = 1$ in Eq. (4.11). The corresponding angle between the inner and the outer inversion spheres can also be calculated and is $\frac{\pi}{3}$ too. This is a favorable coincidence which leads to an allowed initial configuration for constructing a packing. For this reason we obtain a packing based on the tetrahdron which is nothing other than the classical Apollonian packing in three dimensions.

Figure 4.15 shows the initial configuration and Fig. 4.16 shows the packing based on the tetrahedron including all spheres with radii larger than 2^{-7}. Only the spheres in the lower hemisphere are drawn for a more revealing view. Figure 4.17 and Fig. 4.18 show two different cuts of this packing.

For the tetrahedron-based packing five colors are needed such that no spheres having the same color touch each other. Because, any initial sphere touches all others, including the spherical shell. Therefore, each sphere should take a distinct color.

This packing can be constructed alternatively using, so-called, *Soddy* algorithm [74]. There one starts also with four mutually touching spheres on the vortices of a tetrahedron inside the unit sphere. The packing is constructed by putting the biggest possible spheres in the holes between any four spheres which are mutually touching. Equation (3.1) gives the radii of the new spheres. The resulting packing is exactly the same as what we obtained using the inversion algorithm.

4.3.2 Packing based on the octahedron

Here we consider the octahedron as the base for the initial configuration. In this case, there will be six initial spheres on each vortex and eight inversion spheres corresponding to each face of the octahedron. The centers of the inversion spheres are on the vortices of a cube which is conjucate to the octahedron. Considering this, one can easily verify that the angles between the outer inversion spheres is $\frac{\pi}{4}$ which corresponds to $l = 2$ in Eq. (4.11). One can show that

the angle between the inner inversion sphere and the outer ones has also the same value. This is another favorable coincidence which allows us to obtain the first previously unknown packing of spheres.

Figure 4.19 shows the initial configuration and Fig. 4.20 shows the packing based on the octahedron. Figure 4.21 and Fig. 4.22 show two different cuts of the same packing.

In this case, at least four colors are needed for coloring the spheres such that no two spheres having the same color touch each other. This is because each pair of the initial spheres which lay on opposite vortices of the octahedron don't touch each other and can be assigned with the same color. Since there are three such pairs and the unit sphere needs also to be colored distinctly, at least four colors are necessary.

4.3.3 Packing based on the cube

As the third Platonic Solid, we choose a cube as the base for the initial configuration. This time, there will be nine initial spheres, including the unit sphere, and seven inversion spheres. The centers of the outer inversion spheres are on the vortices of an octahedron. In this case, the angle between the inversion spheres is also $\frac{\pi}{3}$ as in the case of the tetrahedron, since an octahedron has triangular faces. So, also in this case the initial configuration fulfills the packing condition and the inversion algorithm will produce a packing.

Figure 4.23 shows the initial configuration and Fig. 4.24 shows the packing based on the cube. Figures 4.25 and Fig. 4.26 show two different cuts of this packing.

For this configuration at least three colors are needed such that no spheres having the same color touch each other. This is because for a cube there are two sets of vortices which are not neighbours, and all corresponding initial spheres can be assigned with a same color. Together with a color for the unit surrounding sphere, at least three colors are necessary.

4.3.4 Packing based on the dodecahedron

The next Platonic Solid which we will consider here as the base for the initial configuration is the dodecahedron. As seen from Fig. 4.27, a dodecahedron has twenty vortices. Therefore, the number of the initial spheres is twenty one,

including the unit sphere. The Platonic Solid conjugate to the dodecahedron is the icosahedron which has twelve vortices. Therefore, there will be twelve outer inversion spheres and one inner one perpendicular to all twenty initial spheres on the votices of the dodecahedron.

The icosahedron which is in this case the base of the inversion spheres has also triangular faces. Therefore, they overlap as shown in Fig. 4.13 and their intersecting angle is $\frac{\pi}{3}$ which corresponds again to $l = 1$ in Eq. (4.11). One has also the same value for the angle between the inner inversion sphere and the outer ones. Therefore, the packing conditions are also fulfilled for this configuration and a packing is expected to be obtained.

Figure 4.27 shows the initial configuration and the resulting packing is shown in Fig. 4.28. It can be shown that in this case at least four colors are necessary for coloring the spheres. Of course, the initial spheres cannot be colored symmetrically with three colors such that there will be the same number of spheres of each color. Looking at Fig. 4.27, there are seven red, seven blue, and six green spheres. The unit sphere is colored with yellow.

4.3.5 Packing based on the icosahedron

So far for each Platonic Solid a packing has been obtained using the inversion algorithm. The overlapping condition was, however, fulfilled automatically by the geometry of the Platonic Solids. These fortunate coincidences may be expected to occur also for the last Platonic Solid, i.e., the icosahedron. But, it turned out to not be the case, as we will discuss here.

Similar to the previous cases, we set up the initial configuration by putting twelve initial spheres, corresponding to the vortices of the icosahedron, inside the unit sphere. The inversion spheres are set in such a way that the first two of the packing condition are fulfilled. There will be twenty outer inversion spheres centered at the votices of a dodecahedron. One more inversion sphere is set at the center, perpendicular to all twelve initial spheres.

The third condition is still to be checked by calculating the angles between the inversion spheres. This can be easily done with the help of Fig. 4.14 which shows the cross-section of five neighbouring inversion spheres with the plane containing their centers. As can be seen, the angle between two adjacent spheres is $\frac{2\pi}{5}$. This value, however, does not match any value of α in Eq. (4.11). This is enough to say that this initial configuration will not give us a packing. Therefore,

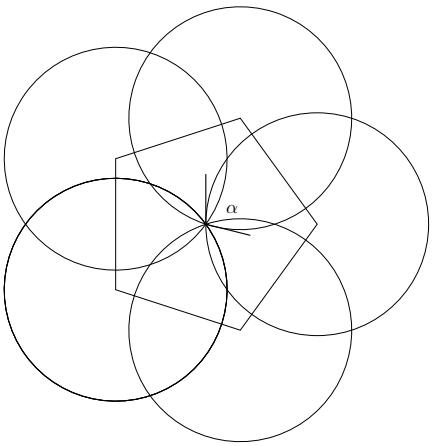

Figure 4.14: Overlapping of the inversion spheres in the case of the icosahedron. α equals $\frac{2\pi}{5}$.

the icosahedron geometry fails to contribute to expand our collection of the new packings of spheres.

4.3.6 Further packings of spheres

Here, we look for further possible initial configurations which may lead to a three dimensional packing. In Sec. 4.2.2 we discussed the generalization of having non-touching initial circles. This may also be applied to three dimensions. Similar to two dimensions, we reduce the size of the initial spheres so that they are not touching each other but still touching the unit sphere. The outer inversion spheres will still be the same as before. But, one needs to expand the inner inversion sphere in order to fulfill the first two of the packing conditions. This will increase further the overlapping of the inner inversion sphere with the outer ones. But, according to Eq. (4.11) one can see that the overlapping of the inversion spheres are at their maximum for all cases we discussed, except for the case of the octahedron for which $\alpha = \frac{\pi}{4}$. In this case the only value of α which leads to an expanded inner inversion sphere and does not deviate from Eq. (4.11) will be $\frac{\pi}{3}$ corresponding to $l = 1$. It should be noted that for $l = 0$ the inner inversion sphere will be as big as the unit sphere and the size of the initial spheres becomes zero, as we will discuss later. Apparently, this initial configuration will not result

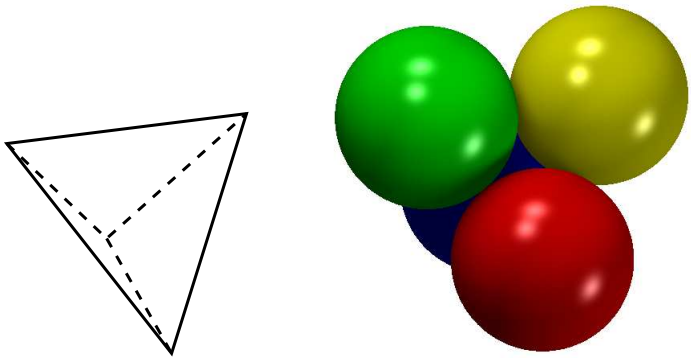

Figure 4.15: Initial spheres are placed on the vortices of a tetrahedron.

in a packing.

Therefore, with this technique only one new packing can be obtained. Figure 4.29 shows the obtained packing together with its first iteration (the image on the left).

Interestingly, for this configuration only two colors are necessary for coloring the spheres such that no two spheres having the same color touch each other. This is because the initial spheres do not touch each other and can be all assigned with the same color. The second color goes to the unit sphere. We refer to this kind of packings as bichromatic. Fig. 4.29 presents the first ever constructed bichromatic space-filling packings of spheres.

As we will discuss in details in the next chapter, being bichromatic is the necessary and sufficient condition for a packing to act as a bearing, where the spheres can rotate, rolling on each other without slip.

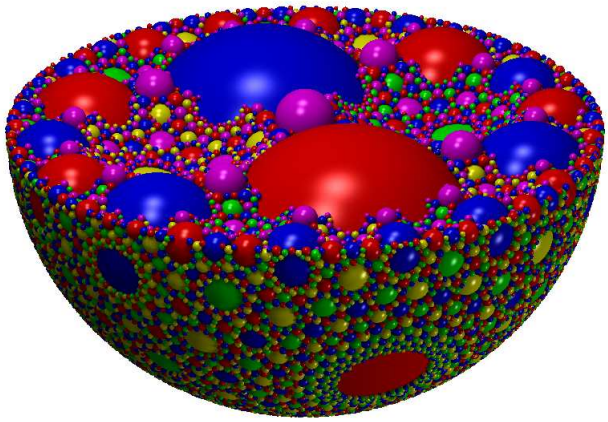

Figure 4.16: The tetrahedron-based packing.

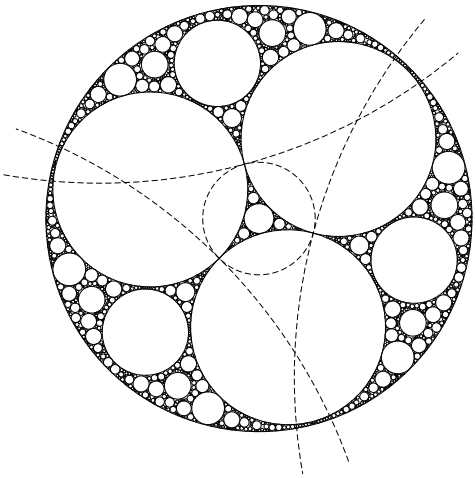

Figure 4.17: Tetrahedron-based packing: Cut of the plane of one of the faces.

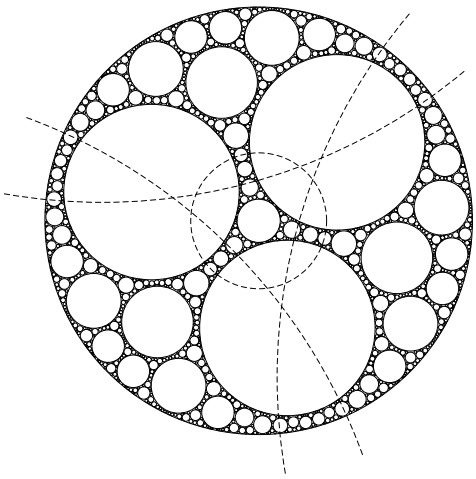

Figure 4.18: Tetrahedron-based packing: Cut of the plane parallel to one of the faces, with the distance of 0.5 from the center of the unit sphere.

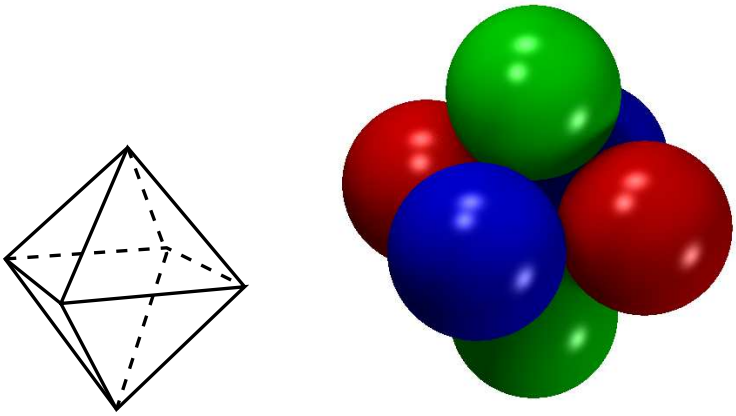

Figure 4.19: Initial spheres are placed on the vortices of a octahedron.

4.4 Fractal dimensions

As we mentioned before, the obtained packings have self-similar structures, and, therefore, are fractals. The method we use to calculate the fractal dimensions

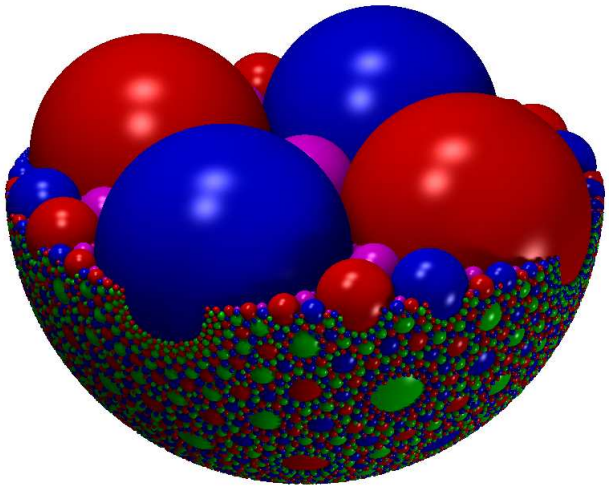

Figure 4.20: The octahedron-based packing.

is the same as the one used in Ref. [73], as already discussed in Ch. 2. The number of all spheres in a packing with radii larger than ϵ follows an asymptotic relation[71, 72],

$$N(\epsilon) \sim \epsilon^{-d_f}, \tag{4.13}$$

in which d_f is the fractal dimension of the packing. Figure 4.30 shows $N(\epsilon)$ in logarithmic scales for different packings. One can see that, for smaller ϵ's the curves become linear the slope of which determines the fractal dimension of the corresponding packing. The slope is calculated by linear fitting to an interval containing five points and shifting this interval towards smaller ϵ's. The results are shown in the inset of the figure.

The difference between the fractal dimensions emphasises the topological difference of the obtained packings. The numerical precision is improved until this difference becomes evident. The fractal dimension of the packing based on the tetrahedron has been calculated in Ref.[74] to a high degree of precision. It is approximately 2.474, which is shown in the figure as the lowest value.

We also calculate the fractal dimensions of two cuts of the bichromatic packing;

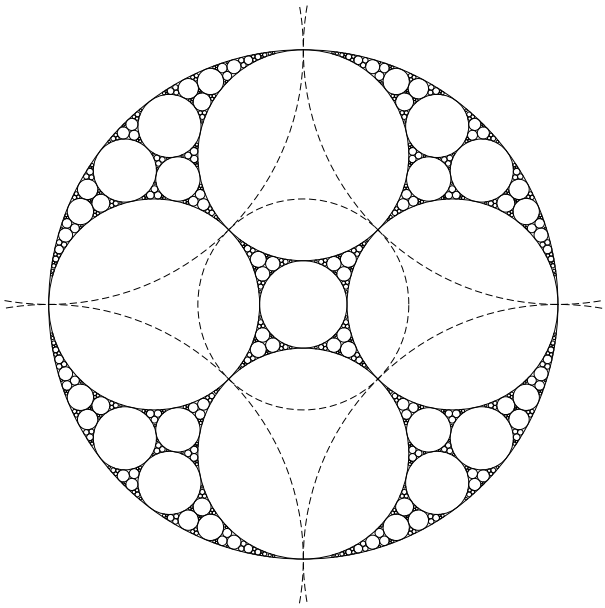

Figure 4.21: Octahedron-based packing: Cut of the plane through the center of the unit sphere.

one through the plane containing four vortices of the octahedron, which also passes the center, and another parallel to this plane but 0.5 off the center. The result is shown in Fig. 4.31. The difference between the fractal dimensions of the cuts shows that the packing is a non-homogeneous fractal. A non-homogeneous fractal is a fractal structure to which more than one dimension can be attributed.

4.5 Stripe geometry

The packings we obtain using the inversion algorithm in two dimensions turn out to be the same as those constructed and named as first family of space-filling bearings by Herrmann et al [32] with $m = N - 3$ and $n = l + 1$ in their nomenclature. As an example, Fig. 4.12 corresponds to $m = 0$, $n = 0$ as they classify it. This can be easily verified by transforming the circular geometry to the stripe geometry.

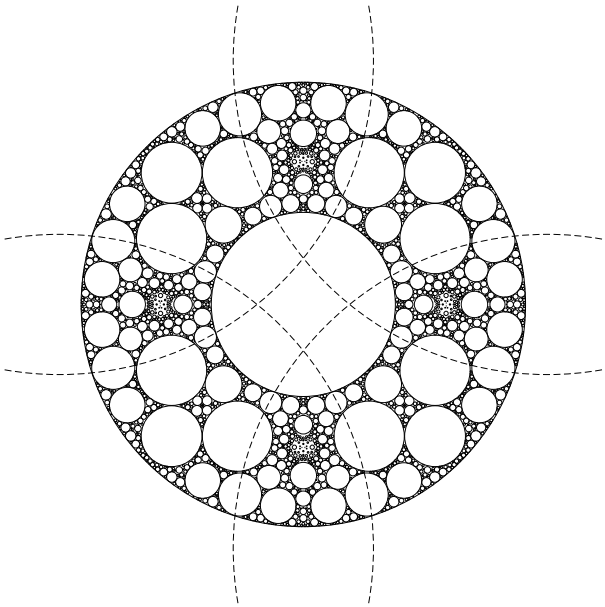

Figure 4.22: Octahedron-based packing: Cut of the plane with the distance of 0.5 from the center of the unit sphere.

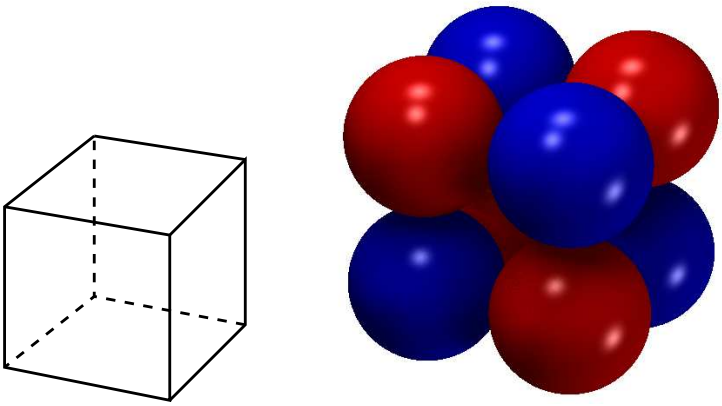

Figure 4.23: Initial spheres are placed on the vortices of a cube.

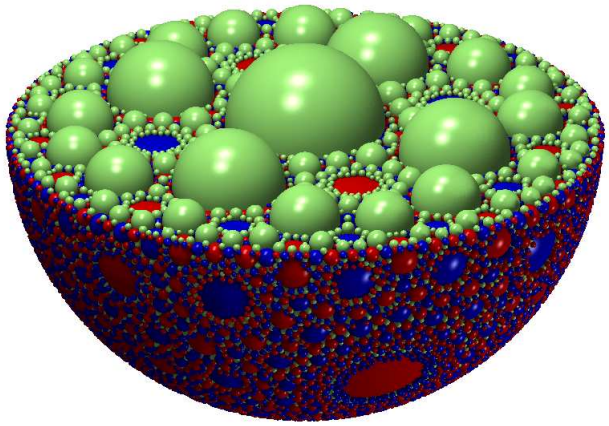

Figure 4.24: The cube-based packing.

Figure 4.32 shows how the circular geometry can be transformed to the stripe geometry. The lower image is the result of the inversion applied on the upper configuration around the inversion circle shown as dashed. The inversion circle can be any circle centered at the touching point of any two circles in the configuration, with no restriction on its radius. The straight parallel lines are the images of these two circles.

All these packings are deterministic, self-similar fractals with a dimension which is different for different n and m. The configurations from the second family of the space-filling bearings can be also constructed using the inversion algorithm. In next section we will discuss more possibilites for choosing the initial configuration in order to obtain further packings in two and three dimensions, including the packings from the second family.

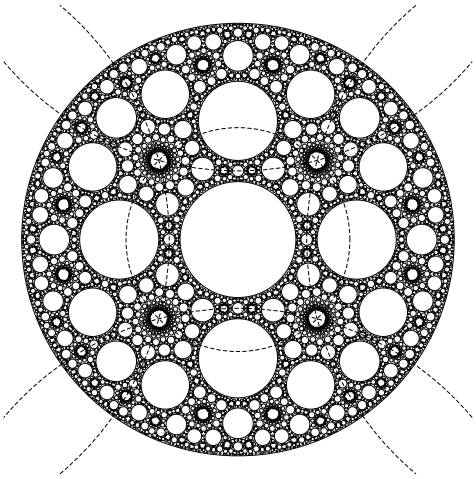

Figure 4.25: Cube-based packing: Cut of the plane through the center of the unit sphere.

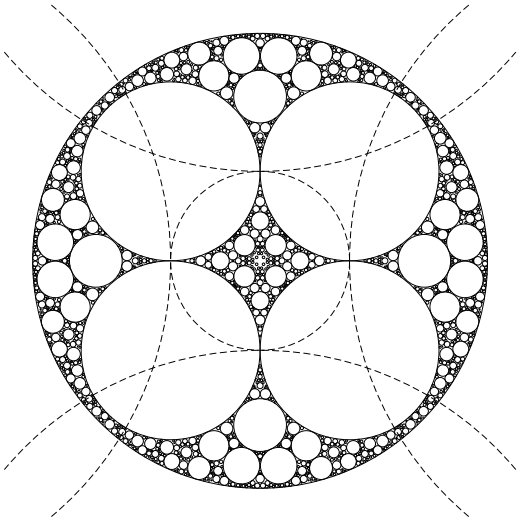

Figure 4.26: Cube-based packing: Cut of the plane of one of the faces.

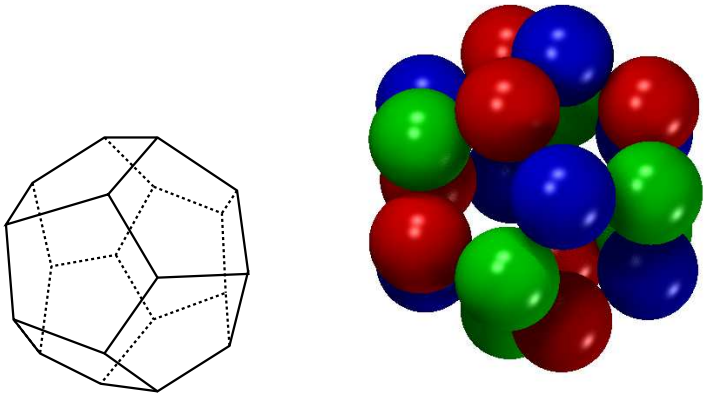

Figure 4.27: Initial spheres are placed on the vortices of a dodecahedron.

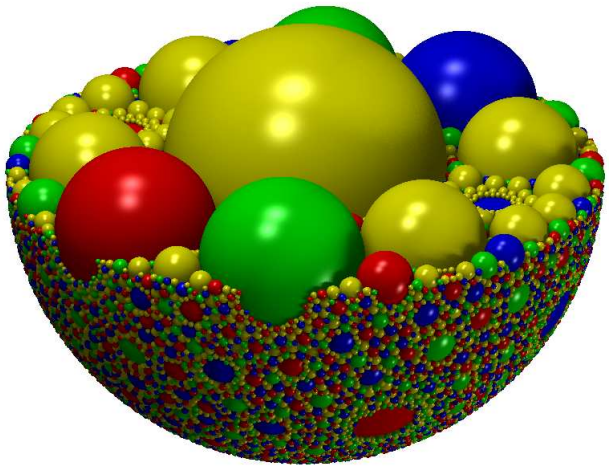

Figure 4.28: The dodecahedron-based packing.

4.6 More packings using the inversion algorithm

As it was discussed before, using the inversion algorithm, the problem of constructing new packings reduces to choosing proper configurations of initial and

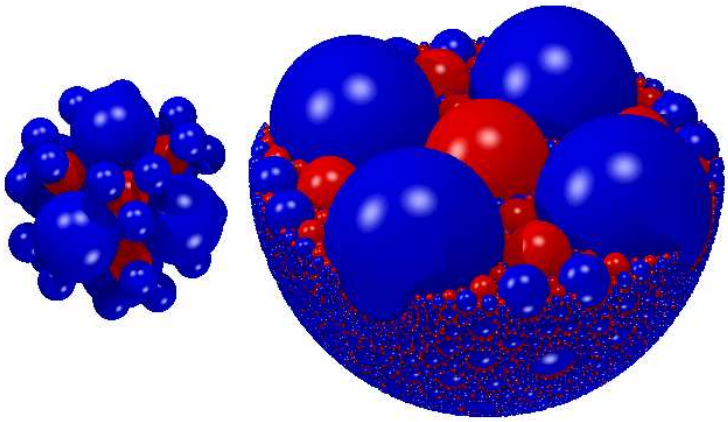

Figure 4.29: The bichromatic packing which is the second octahedron-based packing. No spheres of the same color touch each other.

inversion spheres which fulfill the packing conditions. Here, we discuss some of these choices and present one example.

In all the previous configurations the outer inversion spheres are perpendicular to the initial spheres as one of the packing conditions. One can, therefore, replace any or all of the initial spheres by inversion spheres of the same sizes and centers, since the perpendicular inversion spheres are allowed by Eq. (4.11). The only initial sphere which should not be transformed to an inversion sphere is the unit sphere, otherwise it would be like having many mirrors without having any object. Therefore, depending on the number of the initial spheres, a variety of different new configurations can be obtained in both two and three dimensions.

So far, in any initial configuration, one inner inversion sphere is set at the center. This is, however, not necessary and it is possible to replace this centeral inner inversion sphere by other inner inversion spheres. One example in two dimensions is as follows; Four inner inversion circles of redius 0.5 are set on the vortices of a square inside a unit circle such that all intersect each other at the center of the

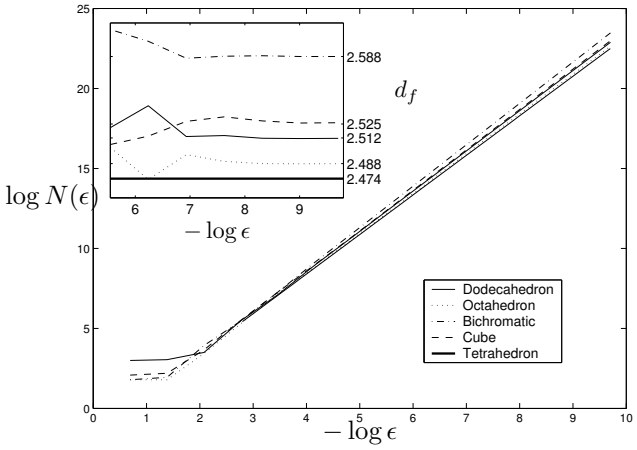

Figure 4.30: The fractal dimension of different packings of spheres.

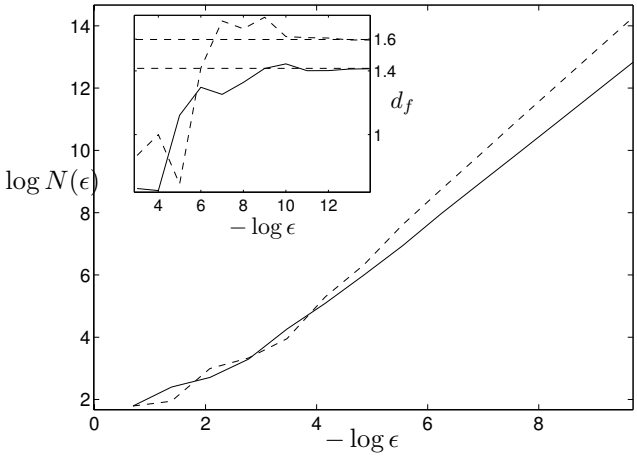

Figure 4.31: The fractal dimension of two cuts of the bichromatic packing.

unit circle. To cover the uncovered space, four outer inversion circles are set as we did in previous section. It can be verified that this configuration fulfills all the packing conditions. The obtained packing is the one corresponding to $m = 1$ and $n = 1$ from the second family of the space-filling bearings, which is shown in Fig. 4.33. For the packings corresponding to other values of m and n one

Platonic Solid	Initial Spheres	Inversion Spheres	Colors	d_F	Bearing
Tetrahedron	5	5	5	2.474	NO
Octahedron(1)	7	9	4	2.488	NO
Octahedron(2)	7	9	2	2.588	YES
Cube	9	7	3	2.525	NO
Dodecahedron	21	13	4	2.512	NO
Icosahedron	13	21	-	-	-

Table 4.1: Summary of the three dimensional packings obtained using the inversion algorithm.

can change the radii of the inner inversion circles in any way which satisfies Eq. (4.11).

4.7 Conformal mapping in the complex plane

As discussed in previous sections, the inversion is a transformation which, although changes the proportions, it keeps the angles unchanged. In two dimensions, this reminds us of Möbius maps which are the general conformal transfomations in the complex plane. Generally, a Möbius map takes the following form:

$$T(z) = \frac{az + b}{cz + d}, \tag{4.14}$$

where z is the coordinate of a point in the complex plane and a, b, c and d are all real numbers. This is the general combination of *magnifications, rotations, translations, reflections,* and *inversions*[2] which are all conformal mappings.

[2]Here, the inversion means $z \mapsto 1/z$ which is a combination of a usual inversion, which we used throughtout this chapter, and the reflection around the real axis.

Indra's Pearls [76] is a beautiful book which is devoted strictly to the properties of these transformations and their use for constructing some interesting patterns including packings of circles.

4.8 Conclusions

We developed an algorithm for constructing self-similar space-filling packings in two and three dimensions. Using this algorithm and its extentions, several previously-unknown packings of spheres have been constructed. These packings are topologically different since they possess different fractal dimensoins. Using a coloring scheme that we introduced, the differences between the packings become even more obvious. Among the three dimensional packings, there is one in which the spheres can be colored with only two colors such that no spheres having the same color touch each other. This is a significant property since it leads to the possibility of rotating spheres with no frustration and therefore to space-filling bearings of spheres, as will be shown in next chapter.

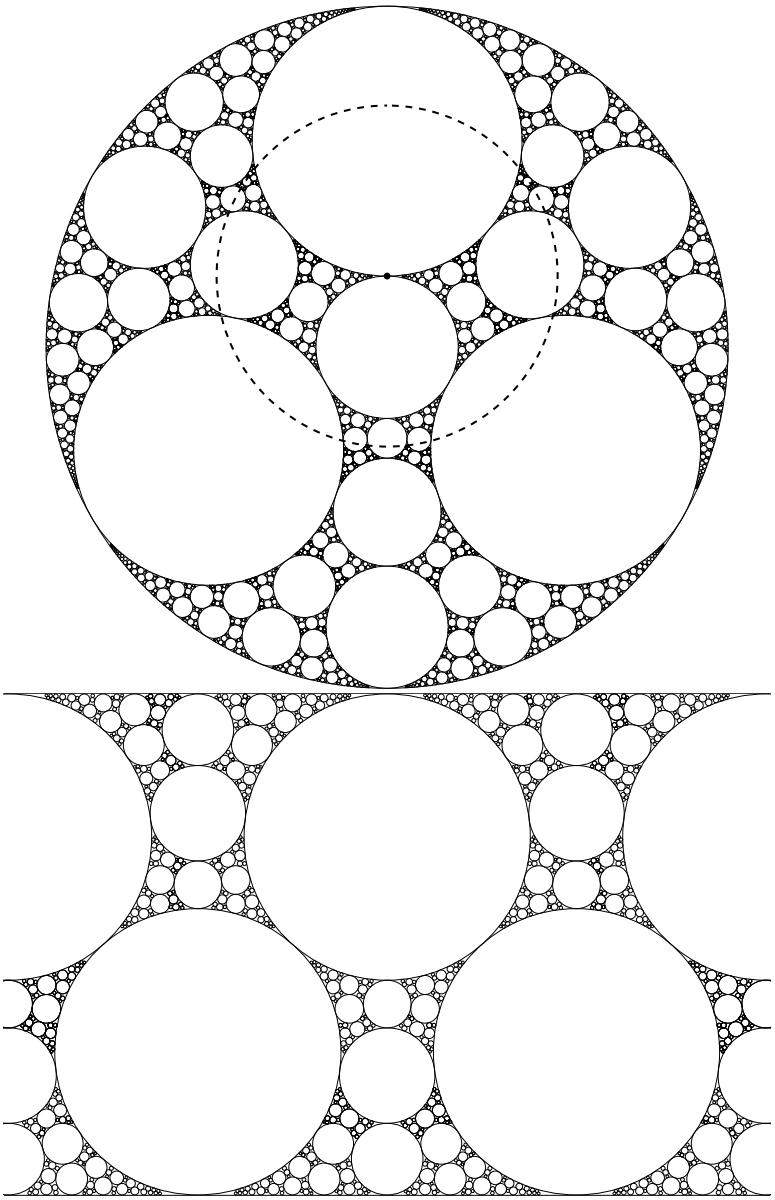

Figure 4.32: Transformation from the circular geometry to the stripe geometry. The lower image is the result of the inversion applied on the upper configuration around the inversion circle shown as dashed. The inversion circle can be any circle centered at the touching point of any two circles in the configuration.

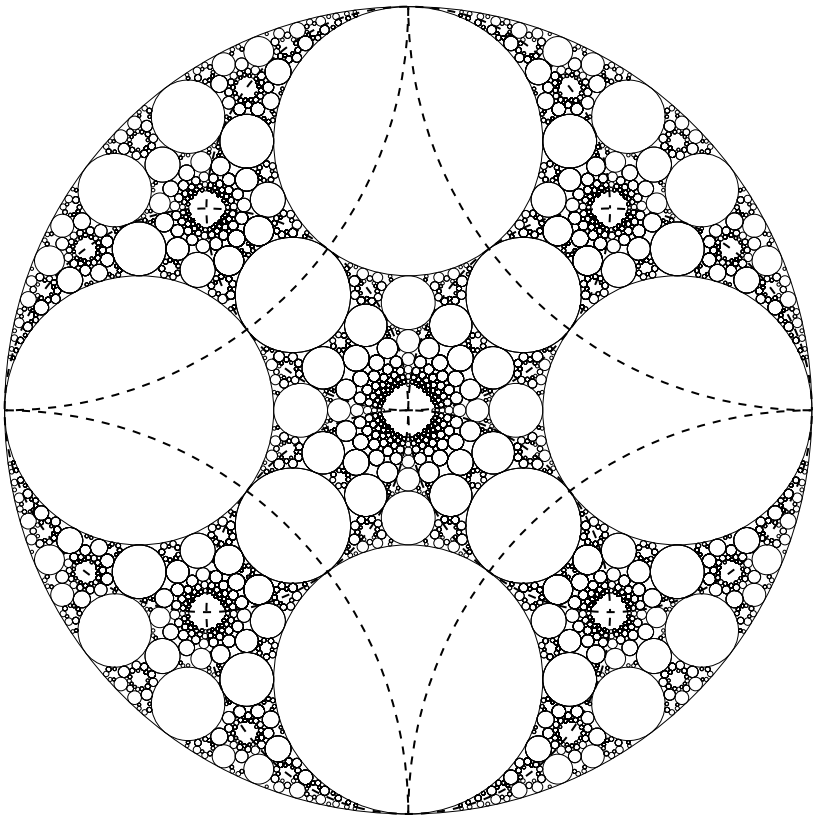

Figure 4.33: Packing corresponding to $m = 1$ and $n = 1$ from the second family of the space-filling bearings. The inversion circles are shown as dashed.

Chapter 5

Space-filling bearings

As discussed in Sec. 3.3, space-filling bearings have some important applications. They can be used for modeling phenomena such as seismic gaps and turbulance. Although in two dimensions a variety of realizations have been constructed, it is not obvious whether they can exist in three dimensions. In this chapter, we will study the space-filling bearings in two and three dimensions. We will show that in both cases the necessary and sufficient condition for a packing to act like a bearing is to have only *even* loops. We will show also that only one of the three dimensional packings we obtained in the previous chapter can act as a bearing.

5.1 Space-filling bearings in two dimensions

As discussed in previous chapters, in two dimensions different classes of space-filling bearings of disks have been constructed in Refs. [32, 33] by requiring the loops to have an *even* number of disks. The term loop refers to a closed chain of successively touching particles in the packing. The number of particles in the chain is called the loop number. Figure 5.1 represents a typical loop of five discs.

In order that two touching discs can rotate without slip on each other, their tangent velocities at their contact point have to be equal, that is:

$$v_t = r_1\omega_1 = -r_2\omega_2 \tag{5.1}$$

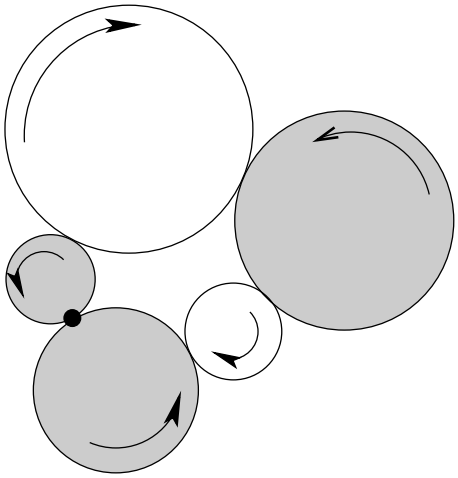

Figure 5.1: Typical loop of discs. For an odd loop there will be at least one frustrated contact, shown as black dot. The colors correspond to the two directions in which the discs rotate. In order to have no frustrated contacts, the loop should be bichromatic (see the text).

where r_1, ω_1, r_2 and ω_2 are radii and angular velocities of the two discs. If the tangent velocities do not agree at the contact point, the discs will slip on each other, and the contact is called frustrated. In a chain of n successively touching discs Eq. (5.1) should hold for each contact if one wants to avoid any frustration, in other words:

$$v_t = (-1)^{i+1} r_i \omega_i \quad i = 1, 2 \cdots n. \tag{5.2}$$

However, for a loop of discs where the chain is closed this is possible only when the loop number n is even. As seen in Fig. 5.1, there will exist at least one frustrated contact, shown as black dot. If the discs are colored according to their direction of rotation, the problem of having a non-frustrated loop reduces to having a *bichromatic* loop, i.e., no two touching discs having the same color touch each other. In other words, being bichromatic is equivalent to having an even loop.

In a loop inside a packing, discs may have more than two contacts. It means that the discs may be member of several loops at the same time. In this case it is also enough to impose the condition of having only even, or equivalently bichromatic,

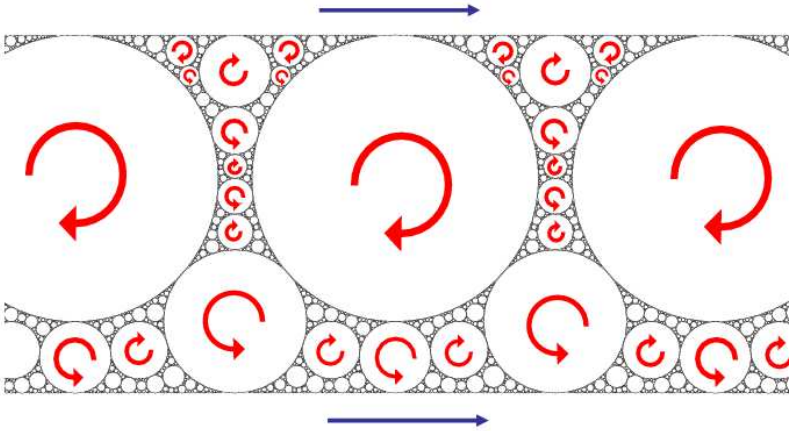

Figure 5.2: Two dimensional space-filling bearing. All discs can rotate without sliding on each other.

loops in order to avoid any frustrated contact. As seen from Eq. (5.2), the tangent velocity at the contact points v_t will be a global constant. All disks must rotate with this velocity, in alternation, clockwise and counter-clockwise, which is possible only in a bichromatic configuration. The different colors correspond to different direction of rotation.

Figure 5.1 shows a rotating space-filling bearing in two dimensions.

5.2 Space-filling bearings in three dimensions

The situation in three dimensions is different from two dimensions in two ways; The axes of rotation need not be parallel, and the centers of the spheres in a loop may not lie all in the same plane. As a result, even in an *isolated* odd loop, spheres could rotate without slip. A simple example is shown in Fig. 5.3. But, as we will see, in the packings with an infinite number of interconnecting loops, one can construct unfrustrated configurations of rotating spheres if all loops have an even number of spheres, i.e., if the packing is bichromatic.

No three dimensional space-filling bearing has been known up to now. The clas-

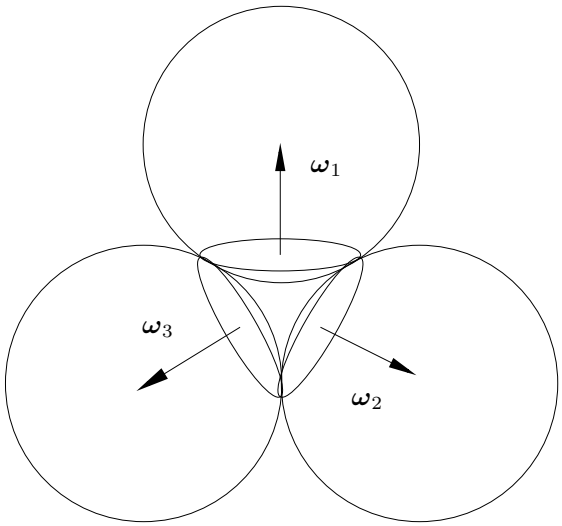

Figure 5.3: Loop of three spheres. In contrary to two dimensions, the spheres can rotate without any frustration even in an odd loop.

sical Apollonian packing is space-filling and self-similar but not a bearing since at least *five* colors are needed to assure different colors at each contact. In Ch. 4 we have shown that three dimensional bichromatic packings exist by constructing one realization (see Fig. 4.29).

As discussed Ch. 4, its construction is based on six non-touching initial spheres on the vortices of an octahedron inside the unit sphere. Figure 5.4 shows the plane cut through the centers of the unit sphere and four initial spheres. Dashed circles are cuts of the inversion spheres. Sphere $S : 0, 1, \cdots$ is mapped, by the inversion sphere shown by a thick dashed line, onto sphere S'. The inversion around this sphere gives no new images of spheres 1 and 2. In the first iteration we make all possible inversions which give new and smaller spheres. In the next iterations, the newly-generated spheres are mapped to smaller spheres. For example, sphere $0'$ is mapped (by the central inversion sphere) onto $0''$. In this way, the remaining empty space is filled in the limit of infinite iterations while the bichromatic topology of the contacts is preserved.

Using our algorithm, the configuration of initial spheres which gives a bichromatic packing is unique. Strictly speaking, it is shown that the only value for radii of the initial spheres which leads to the bichromatic packing without (par-

tial) overlapping of generated spheres is $(\sqrt{3}-1)/2$ and only using an octahedral base (see Ch. 4).

The image on the left of Fig. 4.29 shows the initial configuration and the first generation of inserted spheres, and the one on the right shows the resulting packing containing all the spheres with radii greater than 2^{-7}. The sphere at the center and the external hull is white and those on the vertices of the octahedron are black. Since the spheres on the vertices touch only the external hull and the central sphere, and since this topology is preserved by construction, no two spheres of the same color touch each other.

This implies that every loop of spheres in this packing contains an even number of spheres. We now show that this is a sufficient condition for the spheres in contact to rotate without slip, or even torsion friction.

Consider a loop of n spheres as seen schematically for $n = 4$ in Fig. 5.5. The no-slip condition implies that each pair of touching spheres have the same tangent velocities $\mathbf{v}$ at their contact point. The condition for the contact between the first and the second sphere can be written as:

$$\begin{aligned} & \mathbf{v}_1 = \mathbf{v}_2 \\ \Rightarrow \quad & R_1 \hat{r}_{12} \times \boldsymbol{\omega}_1 = -R_2 \hat{r}_{12} \times \boldsymbol{\omega}_2 \\ \Rightarrow \quad & (R_1 \boldsymbol{\omega}_1 + R_2 \boldsymbol{\omega}_2) \times \hat{r}_{12} = 0, \end{aligned} \tag{5.3}$$

where R_1, R_2, $\boldsymbol{\omega}_1$ and $\boldsymbol{\omega}_2$ are the radii and the vectorial angular velocities of the first and second sphere, respectively. $\hat{r}_{12}$ is the unit vector in the direction connecting the centers of the first and the second sphere. From Eq. (5.3) the vector $(R_1\boldsymbol{\omega}_1 + R_2\boldsymbol{\omega}_2)$ should be parallel to $\hat{r}_{12}$:

$$R_2\boldsymbol{\omega}_2 = -R_1\boldsymbol{\omega}_1 - \alpha_{12}\hat{r}_{12}, \tag{5.4}$$

where α_{12} is an arbitrary parameter. Equation (5.4) is a connection between the rotation vectors $\boldsymbol{\omega}_1$ and $\boldsymbol{\omega}_2$ of the two spheres in contact. Similarly for the third sphere in contact with the second, we have

$$R_3\boldsymbol{\omega}_3 = -R_2\boldsymbol{\omega}_2 - \alpha_{23}\hat{r}_{23}. \tag{5.5}$$

Putting Eq. (5.4) into Eq. (5.5) we find the relation between the angular velocities of the first and third sphere:

$$R_3\boldsymbol{\omega}_3 = R_1\boldsymbol{\omega}_1 + \alpha_{12}\hat{r}_{12} - \alpha_{23}\hat{r}_{23}. \tag{5.6}$$

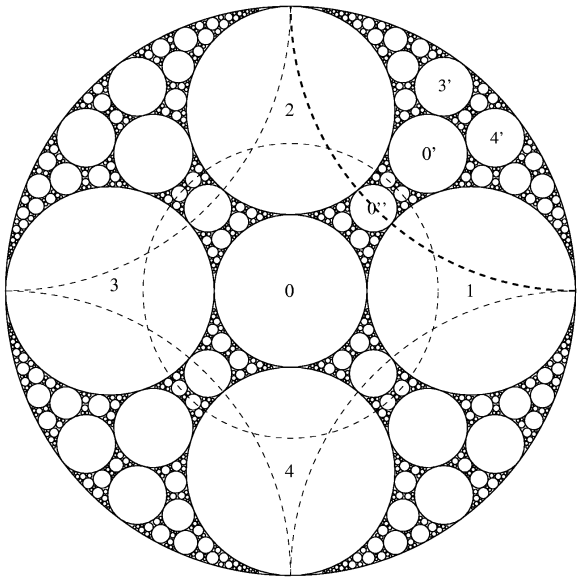

Figure 5.4: Plane cut through the center of the unit sphere and four initial spheres. Dashed circles are cuts of the inversion spheres. Sphere S is mapped, by the inversion sphere shown by a thick dashed line, onto sphere S'. $0'$ is mapped by the central inversion sphere onto $0''$.

In general, we can relate the angular velocities of the first and jth spheres of an arbitrary chain of spheres in no-slip contacts by:

$$R_j\boldsymbol{\omega}_j = (-1)^{j-1}R_1\boldsymbol{\omega}_1 + \sum_{i=1}^{j-1}(-1)^{j-i}\alpha_{i,i+1}\hat{r}_{i,i+1}. \tag{5.7}$$

As long as the chain is open, the spheres can rotate without slip with the angular

velocities given by Eq. (5.7) and no restrictions on $\alpha_{i,i+1}$. But, for a loop of n spheres in contact, spheres j and $j+n$ are identical, so that

$$R_1\boldsymbol{\omega}_1 = (-1)^n R_1\boldsymbol{\omega}_1 + \sum_{i=1}^{n}(-1)^{n-i+1}\alpha_{i,i+1}\hat{r}_{i,i+1}. \tag{5.8}$$

A similar equation holds for every sphere $j = 1, \cdots, n$ in the loop.

Although for a single loop there are many solutions of Eq. (5.8), not all will serve our purpose. In a packing, each sphere belongs to a very large number of loops and all loops should be consistent and avoid frustration. In other words, the angular velocity obtained for a sphere as a member of one loop should be the same as being a member of any other loop.

If the loop contains an even number n of spheres, Eq. (5.8) becomes a relation between the hitherto arbitrary coefficients of connection $\alpha_{i,i+1}$,

$$\sum_{i=1}^{n}(-1)^i\alpha_{i,i+1}\hat{r}_{i,i+1} = 0. \tag{5.9}$$

Using the fact that the loop is geometrically closed:

$$\sum_{i=1}^{n}(R_i + R_{i+1})\hat{r}_{i,i+1} = 0, \tag{5.10}$$

a solution for Eq. (5.9) is

$$\alpha_{i,i+1} = c(-1)^i(R_i + R_{i+1}), \tag{5.11}$$

where c is an arbitrary constant. Putting this in Eq. (5.7), yields the angular velocities

$$\boldsymbol{\omega}_j = \frac{1}{R_j}(-1)^j\left(-R_1\boldsymbol{\omega}_1 + c\mathbf{R}_{1j}\right), \tag{5.12}$$

where $\mathbf{R}_{1j}$ is the vector which connects the centers of the first and jth sphere. As can be seen, the angular velocities only depend on the positions of the spheres, so that the consistency between different loops can be automatically fulfilled provided that the parameter c is the same for every loop of the entire packing.

In Eq. (5.12), all the angular velocities are calculated from $\boldsymbol{\omega}_1$ and c, which can be chosen arbitrarily. ($c = 0$ corresponds to the case when all angular velocities are parallel.)

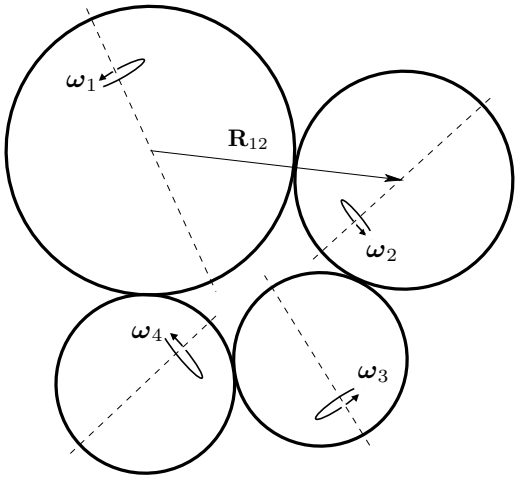

Figure 5.5: Schematic configuration of a loop of four spheres. The spheres rotate without slip. The centers of spheres need not be in the same plane, although $\boldsymbol{\omega}_1$, $\boldsymbol{\omega}_2$ and $\mathbf{R}_{12}$ are coplanar.

The no-slip condition (5.4) then reads

$$R_1\boldsymbol{\omega}_1 + R_2\boldsymbol{\omega}_2 = c\mathbf{R}_{12}, \tag{5.13}$$

so that the vectors $\boldsymbol{\omega}_1$, $\boldsymbol{\omega}_2$ and $\mathbf{R}_{12}$ are coplanar (the plane of Fig.3, containing the two centers and the point of contact A). They are in general not collinear.

We note that the condition of rotation without slip (5.4) also guarantees that there will be no torsion friction, as long as the three vectors are not collinear. Indeed, the locus of the contact point A on sphere 1 is a circle C_1, perpendicular to $\boldsymbol{\omega}_1$. On sphere 2, it is a circle C_2, perpendicular to $\boldsymbol{\omega}_2$. The cone tangent to sphere $i = 1, 2$ on circle C_i has an apex S_i, on the axis $\boldsymbol{\omega}_i$. The two apices S_i are in the same plane as the sphere centers and on the same line as the contact point A (Fig.5.6). The two spheres rolling on each other can therefore be replaced by the two cones rolling on each other, around the line S_1S_2A, which always contains the contact point A. There will be no twisting between cones, thus no torsion friction from one sphere rolling on the other. Only when the two angular velocities and $\mathbf{R}_{12}$ are collinear can there be some twist of the spheres against each other. (The circles C_i then reduce to the contact point A, there are no tangent cones, and the tangent velocities $v_i = 0$). This situation is not generic. It is of measure zero and physically irrelevant.

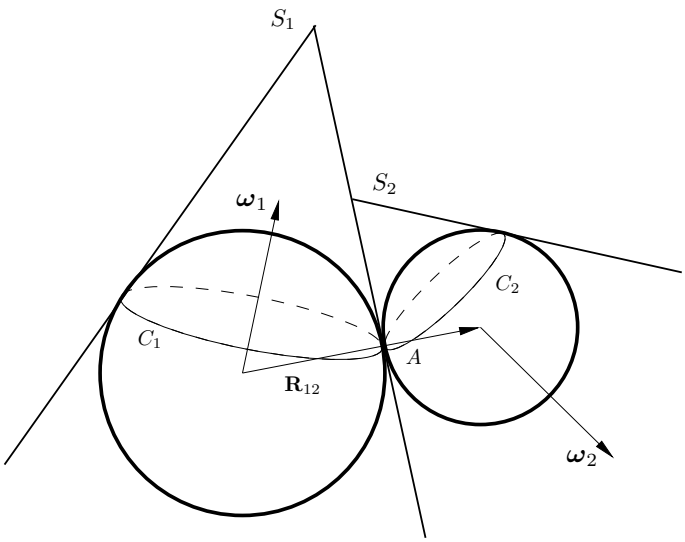

Figure 5.6: Two spheres rolling on each other without slip can be represented by two cones rolling on each other around the common line S_1S_2A. Therefore there is no twist of the spheres against each other.

In the case of odd loops, Eq. (5.8) becomes

$$\sum_{i=1}^{n}(-1)^i\alpha_{i,i+1}\hat{r}_{i,i+1} = 2R_1\boldsymbol{\omega}_1. \tag{5.14}$$

A similar equation holds for every sphere $j = 1, \cdots, n$ in the loop. But, since the coefficients $\alpha_{i,i+1}$ depend then on both geometry and the rotation velocities of the spheres of the loop, consistency between different loops cannot be fulfilled in general and, therefore, a packing containing odd loops cannot be a bearing. A rigorous proof for this, however, is missing. It should be mentioned however that an unfrustrated *single* odd loop is possible, but cannot occur in isolation in a packing [77].

5.3 Conclusions

The bearing discussed here is very idealized and based on exactly-spherical particles with infinite rigidity and, of course, does not exist in this form on all length scales in nature. Nevertheless, chances still remain that similar bearings, though with some imperfections, occur in reality. A simulation of two-dimensional shear bands shows formation of spontaneous rotating bearings in clusters of up to 30 particles [29]. Despite of having more volume, the bearing state is favored because of its low friction. As an another evidence, the bichromatic packing presented here is self-similar which is also observed in the samples of tectonic gouge down to several scales (see Ref. [52]). Interestingly, the measured fractal dimension, 2.60 ± 0.1, agrees with that we obtained in this work.

In summary, we proved the existence of the three dimensional space-filling sphere bearing by presenting the explicit construction. We have shown that a sufficient condition is that the packing is bichromatic, and given an explicit expression (5.12) for the angular velocity of every sphere of the entire packing, in terms of $\boldsymbol{\omega}_1$ and c only. In this way, we support the previous modelization for lubrication between tectonic plates. This result can also be important in mechanics and hydrodynamics.

Chapter 6

Random space-filling bearings

As discussed in the previous chapter, having an even number of particles in all possible loops of a packing is the necessary and sufficient condition for the packing to act as a bearing. In both two and three dimensions, some examples of space-fillings have been presented.

All these configurations consist of highly ordered arrangements of particles. There exists no randomness, whatsoever, in the calculation of the positions and radii of the particles. This is an obvious drawback for a model which is intended to mimic a physical phenomenon. Secondly, in the configurations the space is completely filled with particles of different sizes down to infinitely fine grains, whereas in the reality there exists always a minimum size of the particles.

This chapter is focused on constructing random bearings and studying the effect of cutoffs for the size of the particles on the stability of the system. In the following, an algorithm for constructing random bearings in both two and three dimensions is presented. In the construction procedure, the formation of odd loops is avoided by imposing the bi-chromatic condition. Next, the instability of the configurations as a consequence of setting a cutoff is discussed and calculations for the dissipation of energy in a system with rotating particles under gravity are presented. One can see, that the energy dissipation decreases as the cutoff is reduced. Finally a discussion of the results and the conclusion is given.

The algorithm can be divided in two parts. First we construct a general random packing of discs or spheres. Second we impose the bi-chromatic condition which

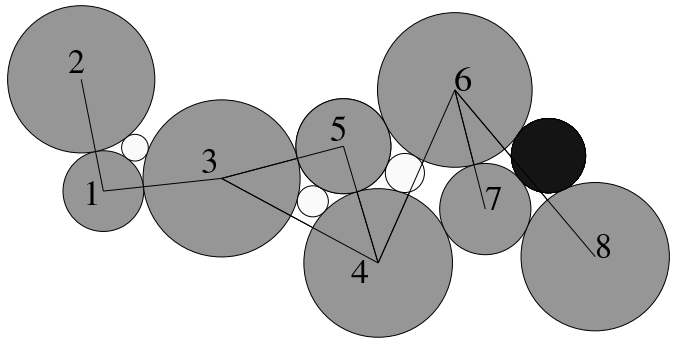

Figure 6.1: The procedure through which a new disc is inserted into the packing. The gray discs are already in the packing. One is randomly chosen (disc 1). We look for the biggest possible disc which can be inserted around disc 1, shown as the empty circle, and set it as the candidate to be inserted next. Then, we look whether it is also the biggest for other touching discs (disc 2 and 3). Continuing this procedure, the final candidate is found, which is shown as a black disc.

implicitly guarantees the packing to contain no odd loops and, therefore, be a bearing.

6.1 Random packing of discs

Initially, some discs within a given range of sizes are randomly distributed in space without touching each other. The filling procedure is continued from then on by inserting always the biggest possible disc into the system without overlapping with any existing disc. This is the most efficient way of filling the space starting from a given initial configuration of discs. This becomes more obvious as the local configurations are observed to be close to that of the classic Apollonian one which is the most efficient known way of packing discs. For finding the biggest hole where a new disc can be inserted, an arbitrary disc A from the current configuration is chosen and all possible neighboring pairs are examined between which a disc can be inserted touching all three without overlapping any other disc in the system. In this way, the locally biggest disc is found and set as the candidate to be inserted next into the system. This disc will touch the initially chosen disc A and two others, namely, B and C. To find the final candidate we check whether the current candidate is also the biggest for B and C. In other

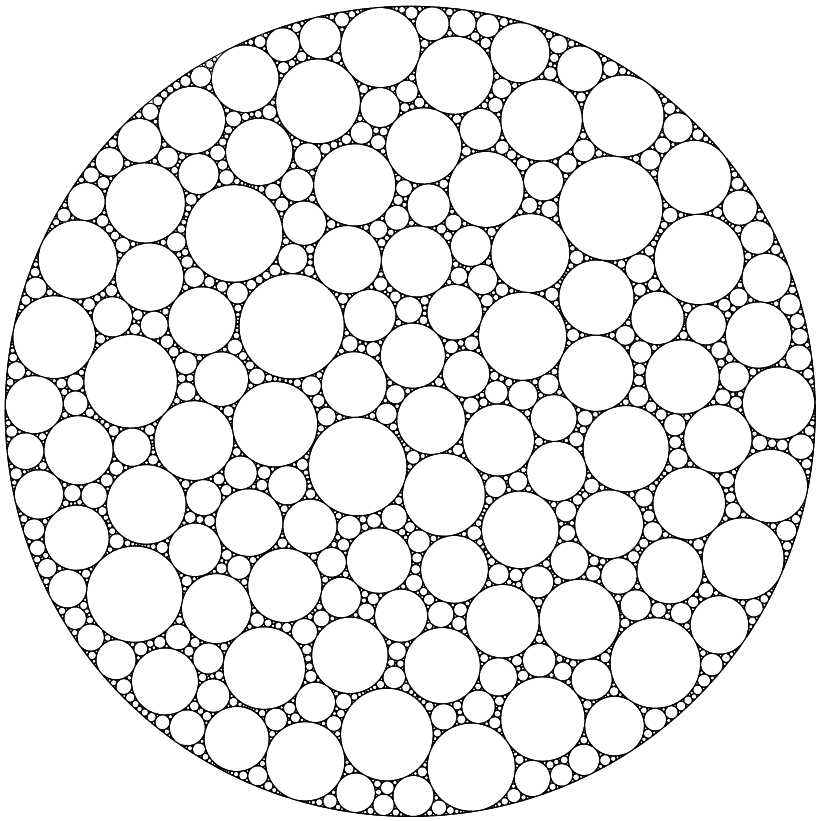

Figure 6.2: A random packing with 2×10^4 discs, and density of 0.99

words, discs B and C are examined as was disc A. If a bigger disc is found the candidate for being inserted next is updated. This is shown in Fig. 6.1. Continuing this search, the biggest disc can be finally found and inserted. More discs are packed into the system by repeating the same procedure over and over. One notices that as the density increases, different regions of the packing become independent. Therefore one doesn't need to look for the globally biggest disc each time and the search can be stopped after a few iterations.

It is worthwhile to have a closer look on how the center and the radius of a circle touching three given circles can be found. In Cartesian coordinates, the equations

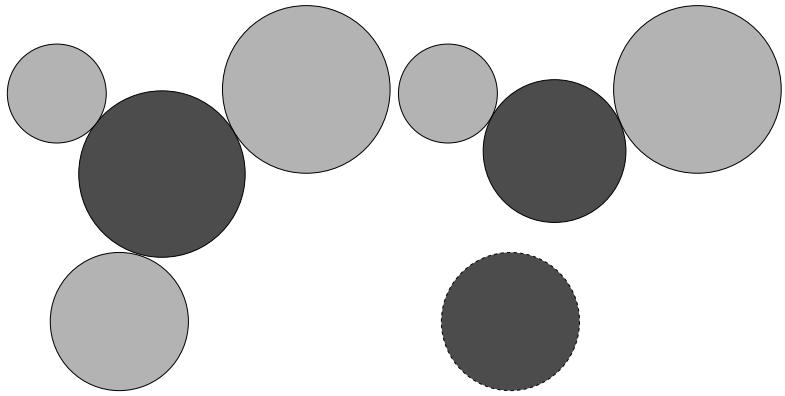

Figure 6.3: The method for construction of a bi-chromatic packing. If all three discs are of the same color (left image) a disc is inserted with opposite color touching all three, otherwise its size is reduced by a factor α so that it only touches the two that have the same color (right image).

governing the distance between the centers are as follow:

$$(x - x_i)^2 + (y - y_i)^2 + (z - z_i)^2 = (r + r_i)^2, \quad i = 1, \cdots, 4 \tag{6.1}$$

where (x_i, y_i, z_i, r_i) are the coordinates of the given spheres, and (x, y, z, r) are the coordinates of the sphere touching all four and which is to be calculated. To solve this system of equations, we subtract the first equation from the other three to get three equations which are linear with respect to (x, y, z). Solving this usual non-homogeneous linear system of equations, coordinates of the center of the sphere (x, y, z) are obtained as functions of radius r. Substituting in the first equation, one gets two different radii, usually one positive and one negative. The positive radius is the desired one since the one with negative radius corresponds to the outer touching sphere.

Figure 6.2 shows the resulting packing with the size of initial circles in the range $0.09 - 0.11$ within a circular space of unit radius.

6.2 Random bearings

So far no considerations have been made for the packing to act as a bearing. As a consequence, there will be many odd loops in the packing which will hinder any

frictionless rotation of the discs. The bearing condition, however, can be easily implemented into the algorithm. The system is initialized as before except that the initial discs are also assigned randomly with two colors. A new disc, gets a color such that it doesn't touch any disc with the same color. This is only possible if all three touching discs have the same color. In other cases, where only two of the discs have the same colors, the radius of the inserted disc is reduced by a factor α with respect to the size which would make it touch to all three:

$$r = \alpha r_0, \tag{6.2}$$

where r_0 is the size of the biggest possible and r is the size of inserted disc as shown in figure 6.3. Obviously, for $\alpha = 1$ we obtain the same packing as in the last section which is not a bearing. Therefore, α must be less than unity in order to have a bearing. Figure 6.4 shows the resulting bearing in two dimensions for $\alpha = 0.6$.

Similarly, random packings and bearings can be obtained in three dimensions with this method. The difference to two dimensions is that each new sphere is inserted touching *four* spheres. To construct a bearing three situations should be considered, that is, among the four spheres one is of one color and three of the other color, two are of one color and two of the other or all three have the same color. Figure 6.7 shows a resulting bearing in three dimensions for $\alpha = 0.6$.

The way we imposed the condition for a bearing, although probably different from what happens in a real or even a simulated system, is a short cut in obtaining a final configuration without considering the dynamics of the particles. One can argue that in an odd loop, when the discs try to rotate, one of the contacts will open and relatively small discs will move between the two discs forming that contact. A spontaneous appearance of bearings in simulations of two-dimensional shear bands has been observed [29]. The simulation of such a system with particles of sizes distributed over several scales, however, still must be achieved.

6.3 Lower bound on the sizes and the stability of the random bearings

From both the computational point of view and that of what happens in reality, a smallest particle size must inevitably exist. The main consequence of this cutoff ε are unfilled spaces which may cause instabilities in the system under external

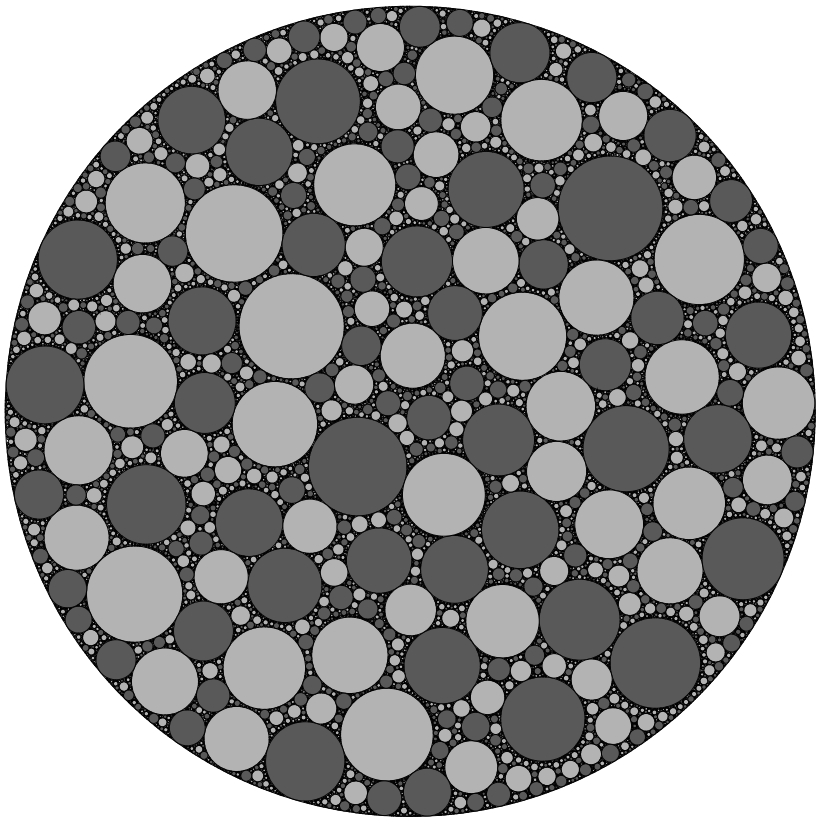

Figure 6.4: Random bearing with $\alpha = 0.6$. For 2×10^4 discs, the density is 0.95.

forces. In other words, the particles may no longer be fixed in their positions, causing changes in the configuration. As we will see, this plays an important role in the dynamics of the bearing. Here in particular we will study the effect of gravity on the system. In a random bearing with a cutoff, the particles which are not supported from below will be displaced by gravity, resulting eventually in the formation of odd loops in the system. In an odd loop at least one frustrated contact will form as the particles are forced to rotate. These are sources for local dissipation of energy and the system will not act as perfect bearing anymore.

The stability of the system depends on how loose it is before applying the gravity. Here, we make an estimate for the total dissipated energy in the system. Assum-

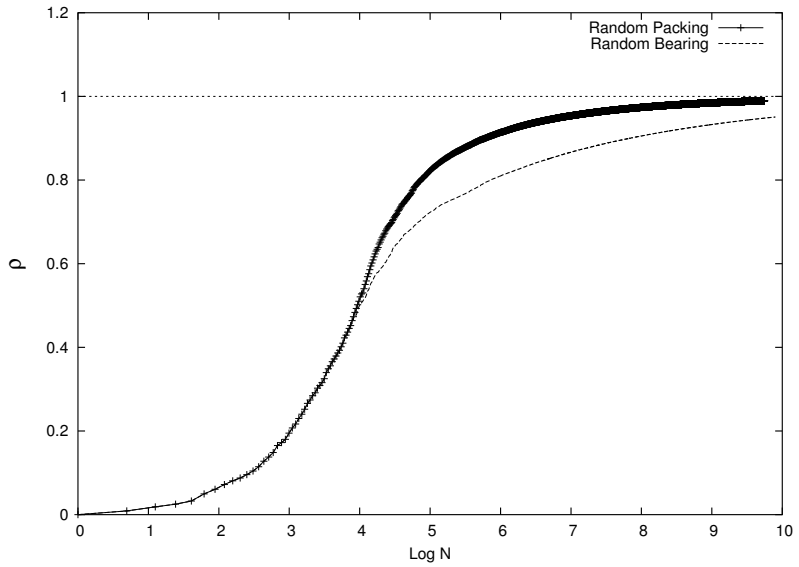

Figure 6.5: Random bearing with $\alpha = 0.6$. For 2×10^4 discs, the density is 0.95.

Figure 6.6: Comparison between the densities of a random packing ($\alpha = 1$) and a random bearing ($\alpha = 0.6$) as function of $\log N$, the total number of discs. In the case of a bearing, the density approaches unity much slower.

ing that the friction acting between two rubbing surfaces follows Coulomb's law, at a frustrated contact, the energy dissipation rate is,

$$\mathcal{E}_{dis} = \mu N v_{rel}, \tag{6.3}$$

where μ is the Coulomb friction coefficient, v_{rel} is the relative velocity of the surfaces of the particles at the frustrated contact, and N is the normal force acting between them. As can be easily verified, the normal force N is proportional to the weight of the dislocated particle. The proportionality factor is a function of the angles between normal forces at the contacts of a particle and the gravity direction. In both two and three dimensions, we assume for all frustrated contacts a typical value for this factor. It should be noted that in two dimensions the relative tangential contact velocity is exactly the same for all contacts, zero for unfrustrated and non-zero for frustrated ones, since all touching pairs of discs can rotate either in the same or in opposite direction. Therefore, we can describe the total dissipation of energy as proportional to the total mass of dislocated particles

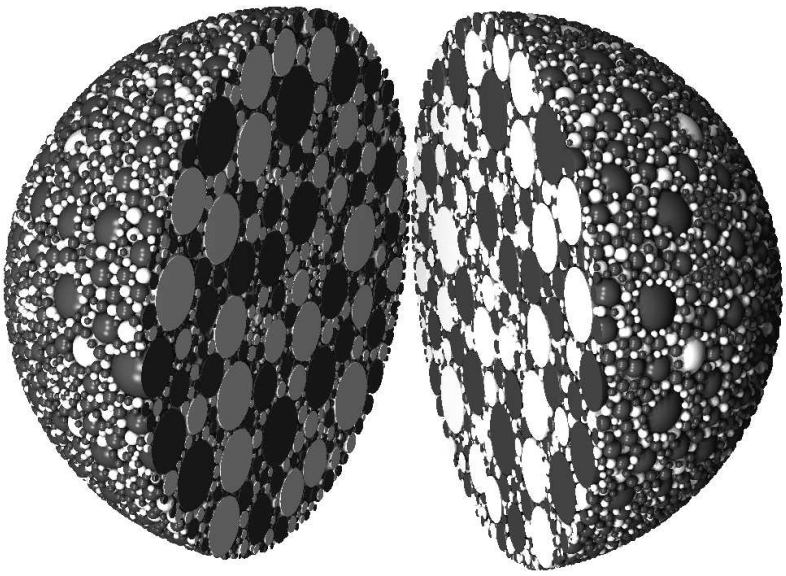

Figure 6.7: Three dimensional random bearing. No two spheres of the same color touch each other.

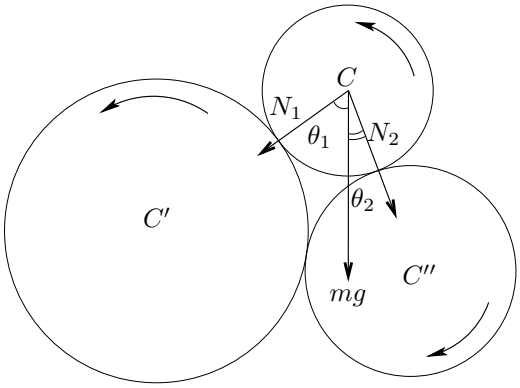

Figure 6.8: A typical odd loop in two dimensions. Particle C hinders the rotation of the other particles and causes some energy dissipation.

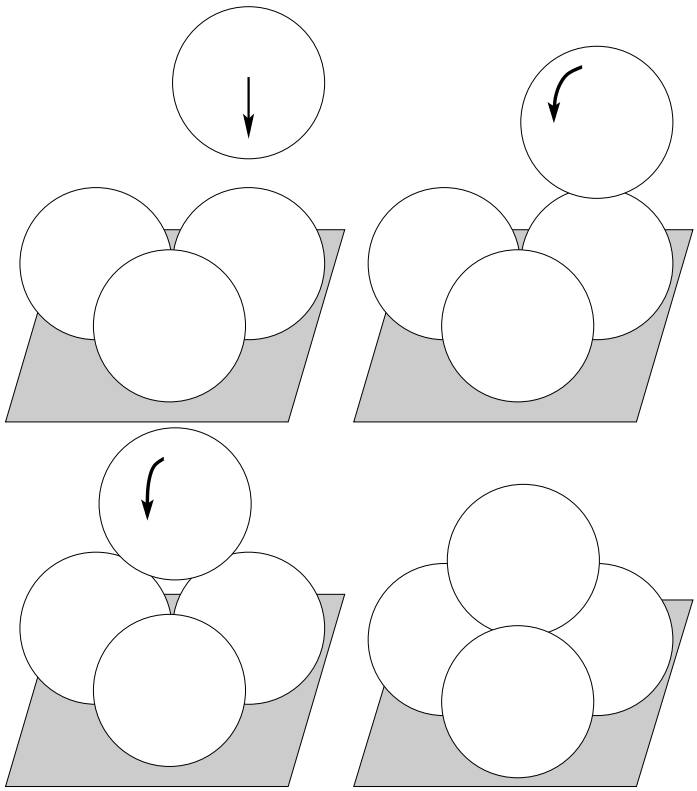

Figure 6.9: Particles fall and roll under gravity until they are fixed through their contacts with other spheres.

that produce frustrated loops:

$$\mathcal{E}_{total} \sim \mathcal{M}, \tag{6.4}$$

which we will consider as the measure for the deviation from a perfect bearing.

To check the effect of gravity on the system, we use a semi-dynamics which is an extension of the one used by Manna et al. [2] to simulate discs under gravity. The particles which do not have enough contacts (at least two in two dimensions and three in three dimensions) to carry their weight will either fall freely or role on one another. All particles are testet one by one from bottom to top and checked whether they are fixed through their contacts with others. If the particle is not

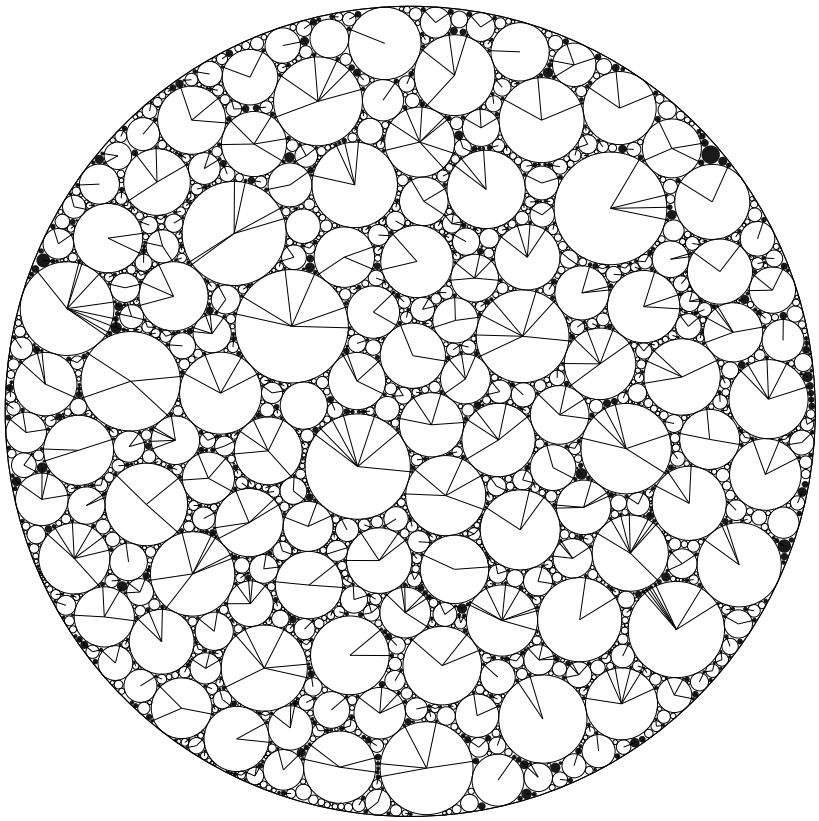

Figure 6.10: Two dimensional random bearing with $\alpha = 0.6$. Applying gravity, some particles move and form frustrated contacts. These are shown as black discs. Solid lines show the frustrated contact.

fixed it either rolls or falls until it hits another one. After a sequence of rollings and fallings, the particle will stop somewhere in the system and stays fixed (see Fig. 6.9.)

A particle is fixed if the line starting at the center of the particle and going in direction of gravity cuts at least one line (triangle) made by connecting two (three) contacts in two (three) dimensions. The process of falling and rolling is performed on all particles one at a time while others are held fixed. Those particles which are in a lower position are treated first and the upper ones later. The pro-

gramm goes through the list of particles several times and lets them fall and roll until no particle moves any more. In this way, the system reaches the final state from which $\mathcal{M}$ the total mass of particles forming frustrated contact can be calculated.

Here, we present the calculation for a two-dimensional system. Figure 6.10 shows a two dimensional random bearing upon which gravity has been applied. Some particles move and form frustrated contacts. These are shown as black discs. Solid lines show the frustrated contacts. The total frustrated mass $\mathcal{M}$ is computed as function of the cutoff ε for different configurations. The result is shown in Fig. 6.11(a) for two values of α. The data points are fitted best by power law functions $\mathcal{M} \sim \varepsilon^{\gamma}$. For different values of α the exponent γ has been calculated, as shown in Fig. 6.11(b).

The results indicate that the system approaches the state of complete stability, that is $\mathcal{M} = 0$, as $\varepsilon \to 0$. Interestingly, for smaller α the total frustrated mass $\mathcal{M}$ is smaller (as seen in Fig. 6.11(a)). For a finite cutoff, there is a finite dissipation on energy which vanishies as the cutoff becomes smaller. The exponent γ has more or less a constant value for the different configurations within the numerical errors, which is 0.72 ± 0.02. This suggests a general behavior for the energy dissipation rate as function of the cutoff for a random bearing.

In the limit $\alpha \to 0$ the configurations are highly polydisperse (see Eq. (6.2)). Whether they still behave like bearings is disputable, since a very small particle between two big particles in reality can very unlikely prevent frustration. On the other hand, in the case of $\alpha = 1$ all the particles are fixed and the configuration is completely stable. However, as was mentioned before, this is the limit where the system becomes fully frustrated due to the formation of many odd loops in the construction stage. Therefore, to study the role of α, we calculate the exponent γ only for the systems with their corresponding α away from these limits (see Fig. 6.11).

6.4 Other properties

In this section, we discuss some properties of different packings which have been generated by the method presented in this chapter. As the most important property of a packing, in Fig. 6.6 the density of two configurations is shown as function of total number of discs. In the case of a random packing, with $\alpha = 1$, the density after the initialization increases faster. This is expected, since imposing

the condition for a bearing we loose some efficiency by reducing the size of those discs which would otherwise form odd loops (see previous section).

As discussed in Ch. 3 the radii distribution $n(r)$ of the discs of such packings follows a power law, as we go to smaller scales. Therefore, a fractal dimension can be assigned to a packing which is related to the exponent of the radii distribution:

$$n(r) \sim r^{-\tau}, \quad d_f = \tau - 1 \tag{6.5}$$

To calculate the fractal dimension, instead of $n(r)$, we use $N(\varepsilon)$ which is the total number of discs with $r > \varepsilon$:

$$N(\varepsilon) = \int_{\varepsilon}^{\infty} n(r)dr \sim \varepsilon^{-d_f} \tag{6.6}$$

This function is shown in Fig. 6.12 in logarithmic scale for the two mentioned configurations. According to Eq. (6.6) the slope is the fractal dimension of the corresponding configuration. After the initialization (omitting the first data point), the slope is is small, about 1.2, even smaller than that of the well-known Apollonian packing in two dimension, ~ 1.306 [73], which has the lowest fractal dimension among all known disc packings. In addition, it can be easily shown that the smaller the fractal dimension the faster the density increases, which may make us believe that in our packing the discs are packed more efficiently than in the Apollonian one. In fact, at the beginning the density increases faster because of our poorly packed initial configuration. We can see that, the slope increases and, for the case of random packings, it seems to approach that of the Apollonian packing. For the case of random bearings, the fractal dimension approaches even a larger value.

Also in three dimensions, we compare $N(\varepsilon)$, the total number of spheres larger than ε, for a random packing ($\alpha = 1$) and a random bearing ($\alpha = 0.6$), which is shown in Fig. 6.13. The slope of each curve is the fractal dimension, 2.37 for the packing and 2.40 for the bearing. Both fractal dimensions are smaller than that of the classical Apollonian packing and also other space-filling packings of spheres (see Ch. 4). We have already discussed a similar situation in two dimensions.

6.5 Conclusions

All space-filling bearings, which have been obtained and studied so far, were highly organized arrangements of particles. This is a drawback for them to model natural phenomena, like tectonic plate motion. Here, we presented an algorithm for producing some space-filling bearings in which the particles do not follow any regular pattern. It is argued that any odd loop will be broken at one of its contacts as the particles try to rotate. Therefore, the spontaneous formation of even loops becomes possible. Such a spontaneous formation of bearings has been observed in simulations of two-dimensional shear bands [29]. We also investigated the stability of the bearing under gravity and showed that as the system becomes more filled the amount of particles which moves and may hinder the motion of the bearing becomes smaller and therefore the system becomes more stable.

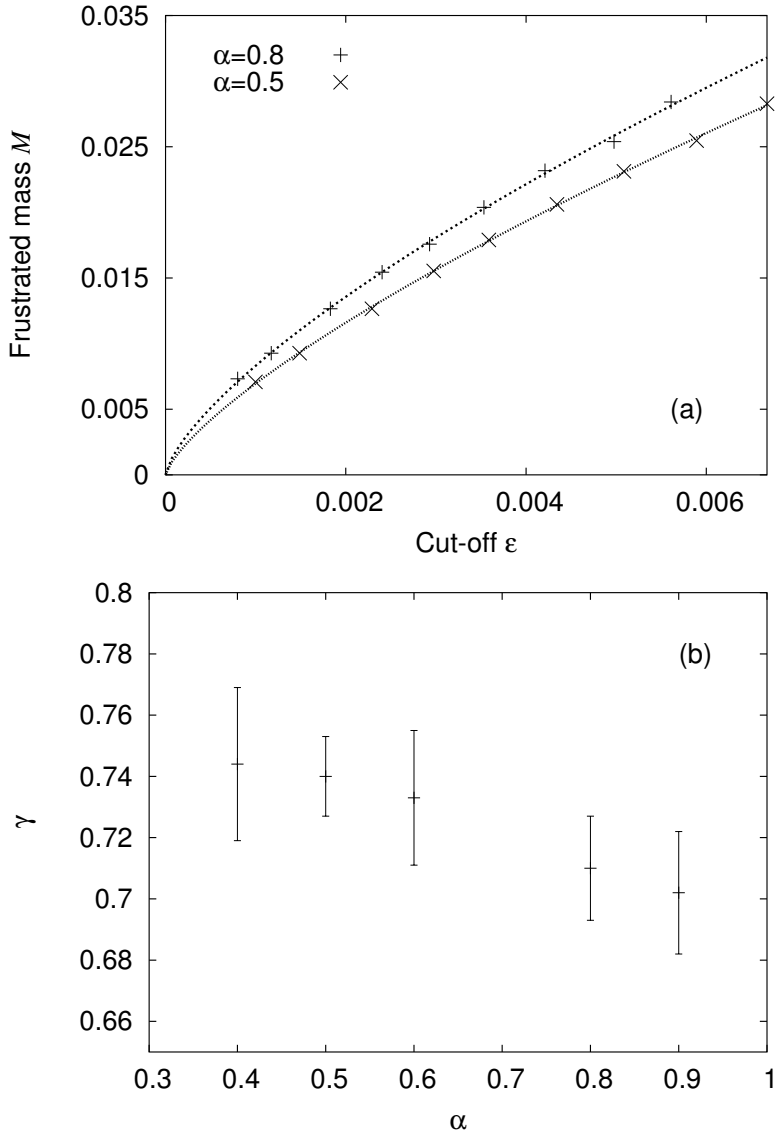

Figure 6.11: (a) Frustrated mass $\mathcal{M}$ as function of the cutoff ε for two dimensional bearings for $\alpha = 0.5$ and 0.8. Lines are different power law fits, with exponents γ=0.74 and γ=0.71 correspondingly. (b) Exponent γ as function of α.

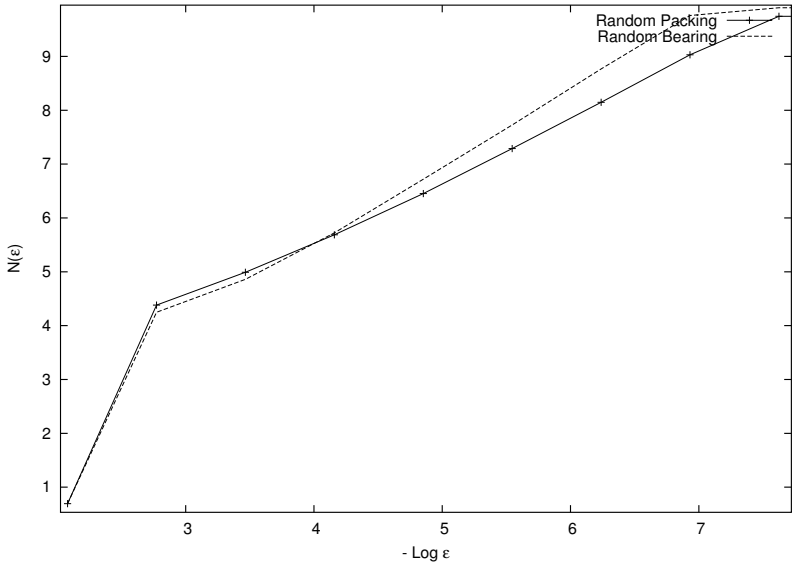

Figure 6.12: Comparison between $N(\varepsilon)$, the total number of discs larger than ε, for a random packing ($\alpha = 1$) and a random bearing ($\alpha = 0.6$). The slope is the fractal dimension.

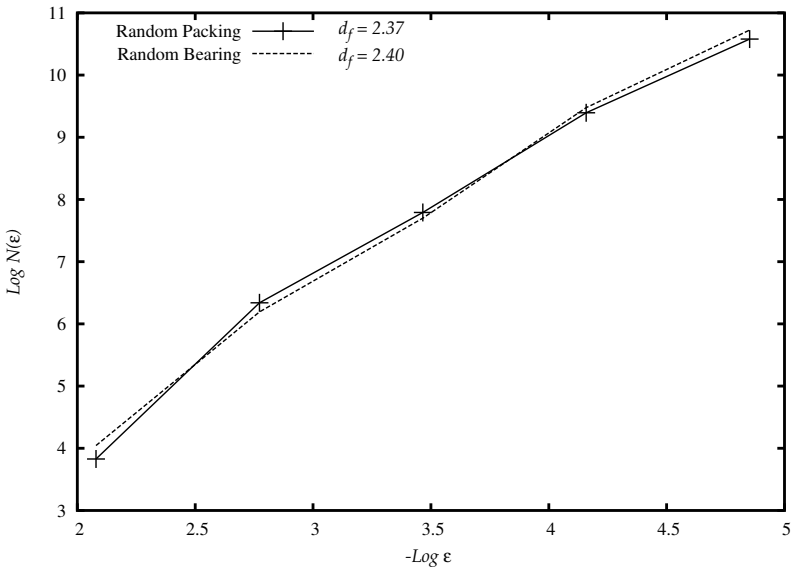

Figure 6.13: Comparison between $N(\varepsilon)$, the total number of spheres larger than ε, for a random packing ($\alpha = 1$) and a random bearing ($\alpha = 0.6$). The slope is the fractal dimension.

Chapter 7

Conclusions

In this thesis we developed an algorithm for constructing three dimensional self-similar space-filling packings of spheres [78–82]. Among the constructed configurations is the classical three dimensional Apollonian packing which was the only previously-known configuration. The difference between the calculated fractal dimensions indicates the topological difference between these configurations. Following a coloring scheme for the spheres, the differences become even more obvious. Although, we did not exhaust all the possible configurations which may be obtained using our algorithm, we have given detailed guidelines useful for discovering further possibilities.

Among the obtained packings there is one for which only two colors are necessary for coloring the spheres such that no two spheres having the same color touch each other. This is equivalent to saying that the packing consists of only even loops of touching spheres. In two dimensions this is the necessary and sufficient condition for a packing to act like a bearing. In three dimensions, however, it is not obvious that this is the case, since the particles have more rotational degrees of freedom. We showed that having only even loops is the necessary and sufficient condition for a packing to act like a bearing in three dimensions as well [83]. We have given an explicit expression (Eq. 5.12) for the angular velocity of every sphere of the entire packing, in terms of $\boldsymbol{\omega}_1$, which is the angular velocity of an arbitrarilily chosen sphere, and a factor $c \geq 0$. All other spheres rotate accordingly. Therefore, there will be infinitely many configurations of rotation axes corresponding to the different values of $\boldsymbol{\omega}_1$ and c versus the two dimensional case where there is only one. For $c = 0$ all the axes are parallel whereas for a

finite value of c the spheres rotate around non-parallel axes.

Space-filling bearings have been introduced in several contexts, such as explaining the so-called seismic gaps [48, 50] of geological faults. The deformation of geomaterials produces well-known spontaneous shear planes. Due to the granular structure inside the shear planes, grains can rotate. In fact, the tectonic faults are examples of shear planes which are spontaneously formed inside the earth's crust. In the upper layers of the earth's crust, where the hydrostatic pressures are not too high, the network of faults has been monitored over many orders of magnitude and self-similarity has been measured by Barton and others [51] from geological maps. Active faults flow on a layer of fragments, called gauge, which over time organizes itself into a size distribution [52] given by a power law. Also rotations have been observed in the gauge zone [48, 53, 54].

As mentioned before, all the obtained packings consist of highly ordered arrangements of particles. There exists no randomness, whatsoever, in the calculation of the positions and radii of the particles. This is an obvious drawback for a model which is intended to mimic a physical phenomenon. We developed a simple method for constructing random bearings in both two and three dimensions.

Another criticism of the space-filling bearings, is the lack of any lower bound for the sizes of the particles. In reality such a lower bound exists for any system and cannot be avoided. We adapted our model to be able to account for this fact by introducing a cut-off for the size of the particles below which no particle is allowed to be inserted into the system. As an artifact of this restriction, there will be many holes throughout the system left unfilled. It will, therefore, not only make sense but also will be crucial to study the stability of such system under external forces. In this work, we studied the effect of the gravity force on different random bearing as function of the cut-off imposed on the size of the particles, using a semi-dynamics in which the full details of the motions of the particles are omitted and only the final configuration is of interest. As expected, the particles which are not supported from below will be displaced by gravity, eventually resulting in the formation of odd loops in the system. In an odd loop at least one frustrated contact will form as the particles are forced to rotate. These are sources for local dissipation of energy and the system will not act as a perfect bearing anymore. We presented a way to calculate the rate of the total dissipation of energy if the particles are forced to have steady rotation. The results show that, for a finite cut-off, there is a finite dissipation on energy which vanishes as the cut-off becomes smaller like a power law function of exponent γ. This exponent has been calculated and seems to be the same for different configurations within the numerical errors, its value being 0.72 ± 0.02. This proposes a general behavior for the energy dissipation rate as function of the cut-off in a random bearing.

Space-filling bearings have also been used as toy models for turbulence and can also be used in mechanical devices [55].

7.1 Outlook

We believe that the present work is a significant step in the subject which opens a horizon for further investigations. The study of space-filling packings and bearings is a young field with a lot of potential for both theoretical and experimental research. Here we discuss some possibilities of what can be done in future.

Regardless of the fact that all the obtained configurations are highly regular which makes them pure geometrical objects, they are all clear examples of the systems with density one. In other words, each configuration presents a size distribution for the spherical particles with which the space can be completely filled at least in one way. This removes any upper theoretical limit on the density for this particular size distribution. This is important in many practical applications. For example, in the fabrication of high performance concretes (HPC) the key is to get to the highest possible densities. If a theoretical limit on density exists, no possible mixing technique gives us a density higher than that limit. The simplest example is the mono-disperse distribution of particles for which the upper limit of the density is about 0.91 for two and 0.74 for three dimensions. Therefore, it is crucial to choose a right size distribution.

In practice the particles are put together using some mixing technique and it is very improbable that a given single configuration can be reached. A statistical approach, therefore, seems inevitable. Whether there is another arrangement with the same size distribution which leads to the density one is unknown. This poses an important question: Given a set of particles, what is the maximum density which can be obtained? Till now, this question has not been studied and answered except in the simplest case where all the particles have the same size.

The random arrangement and the existence of a lower bound for the size of the particles posed the problem of the stability of a bearing. We studied this problem and obtained some results for the energy dissipation rate where the particles are forced to have steady rotations. This problem may also be studied experimentally. The following set up for an experiment is proposed: The space between two concentric cylinders is filled with spherical particles of different sizes. The sizes of the particles may be chosen to be very small compared to the radii of the cylinders. By fixing one of the cylinders and rotating the other one with a constant velocity, the energy dissipation rate can be measured from the amount of the work

per unit time needed for rotating the cylinder. If all the particles are interlocked, the energy dissipation rate will be proportional to the pressure on the cylinders' walls. The proportionality factor is the Coulomb friction coefficient times the velocity of the cylinder. Significant decrease in the energy dissipation rate will be expected due to the formation of local or global bearings behavior in the system.

Chapter 8

Appendix

Here, we derive the inversion matrix in Eq. 4.8 in terms of the inversion coordinates of the inversion sphere.

A sphere can be specified by the coordinates of its center (x, y, z) and its radious r. If the sphere $S' : (x', y', z', r')$ is the image of sphere $S : (x, y, z, r)$ under the inversion about the sphere $S_i(X, Y, Z, R)$, then:

$$\frac{r}{r'} = \frac{x - X}{x' - X} = \frac{y - Y}{y' - Y} = \frac{z - Z}{z' - Z} = \frac{R^2}{d'^2 - r'^2}. \tag{8.1}$$

Defining the inversion coordinates as

$$\begin{aligned} a_1 &= \frac{x}{r}, \;\; a_2 = \frac{y}{r}, \;\; a_3 = \frac{x}{r}, \\ a_4 &= \frac{x^2 + y^2 + z^2 - r^2 - 1}{2r} \\ a_5 &= \frac{x^2 + y^2 + z^2 - r^2 + 1}{2r}. \end{aligned} \tag{8.2}$$

Using Eq. 8.1, we have:

$$\frac{x-X}{r}=\frac{x'-X}{r'}\rightarrow\frac{x}{r}=\frac{x'-X}{r'}+\frac{X}{r}=\frac{x'-X}{r'}+\frac{X}{r'}\frac{d'^2-r'^2}{R^2}\rightarrow$$

$$\frac{x}{r}=\frac{x'-X}{r'}+\frac{X}{r'R^2}\left[(x-X)^2+(y-Y)^2+(z-Z)^2-r'^2-R^22)\right]$$

(8.3)

which can be rearranged to the following form:

$$\begin{aligned}\frac{x}{r}=\frac{x'}{r'} &+ \frac{X}{R^2}\left(\frac{x^2+y^2+z^2-r'^2}{r'}\right)\\ &+ \frac{X}{r'R}\left(\frac{X^2+Y^2+Z^2-R^2}{R}\right)\\ &- 2\frac{X}{R}\left(\frac{x'X+y'Y+z'Z}{r'R}\right)\end{aligned}$$

(8.4)

in other words

$$a_1=a'_1+A_1(A_5-A_4)(a'_4+a'_5)+A_1(A_5+A_4)(a'_4-a'_5)-\\ 2A_1(a'_1A_1+a'_2A_2+a'_3A_3)$$

(8.5)

from which the first coordinate of spheres S and S' can be linearly related:

$$a_1=(1-2A_1^2)a'_1-2A_1A_2a'_2-2A_1A_3a'_3-2A_1A_4a'_4+2A_1A_5a'_5 \quad (8.6)$$

The second and third coordinates can be derived similarily:

$$a_2=-2A_2A_1a'_1+(1-2A_2^2)a'_2-2A_2A_3a'_3-2A_2A_4a'_4+2A_2A_5a'_5 \quad (8.7)$$

$$a_3=-2A_3A_1a'_1-2A_3A_2a'_2+(1-2A_3^2)a'_3-2A_3A_4a'_4+2A_3A_5a'_5. \quad (8.8)$$

For the last two coordinates we begin with:

$$\frac{d^2-r^2}{rR}=-2(a_1A_1+a_2A_2+a_3A_3+a_4A_4-a_5A_5)+\frac{R}{r}$$

on the other hand we have:

$$\frac{d^2-r^2}{rR}=\frac{R}{r'}$$

so we have:

$$\begin{aligned} a_1A_1 + a_2A_2 + a_3A_3 + a_4A_4 - a_5A_5 = - \\ (a'_1A_1 + a'_2A_2 + a'_3A_3 + a'_4A_4 - a'_5A_5) \rightarrow \\ a_5A_5 - a_4A_4 = a_1A_1 + a_2A_2 + a_3A_3 + \\ (a'_1A_1 + a'_2A_2 + a'_3A_3 + a'_4A_4 - a'_5A_5)\,, \end{aligned}$$

using Eqs. (8.6,8.7,8.8) we have:

$$a_5A_5 - a_4A_4 = 2(A_4^2 - A_5^2)\,(a'_1A_1 + a'_2A_2 + a'_3A_3 + a'_4A_4 - a'_5A_5) + a_5A_5 - a_4A_4. \quad (8.9)$$

On the other hand we have:

$$\frac{1}{r} = a_5 - a_4 = 2(A_4 - A_5)\,(a'_1A_1 + a'_2A_2 + a'_3A_3 + a'_4A_4 - a'_5A_5) + a'_5 - a'_4. \quad (8.10)$$

Solving Eqs. (8.9,8.10), we have:

$$a_4 = -2A_4A_1a'_1 + 2A_4A_2a'_2 - 2A_4A_3a'_3 + (1 - 2A_4^2)a'_4 + 2A_4A_5a'_5 \quad (8.11)$$

$$a_5 = -2A_5A_1a'_1 - 2A_5A_2a'_2 - 2A_5A_3a'_3 - 2A_5A_4a'_4 + (1 + 2A_5^2)a'_5. \quad (8.12)$$

Therefore, the inversion coordinates of sphere S are related to those of sphere S' through a linear system of equations which can be shown in the matrix form:

$$\begin{pmatrix} a'_1 \\ a'_2 \\ a'_3 \\ a'_4 \\ a'_5 \end{pmatrix} = \quad (8.13)$$

$$\begin{pmatrix} 1 - 2A_1^2 & -2A_1A_2 & -2A_1A_3 & -2A_1A_4 & 2A_1A_5 \\ -2A_2A_1 & 1 - 2A_2^2 & -2A_2A_3 & -2A_2A_4 & 2A_2A_5 \\ -2A_3A_1 & -2A_3A_2 & 1 - 2A_3^2 & -2A_3A_4 & 2A_3A_5 \\ -2A_4A_1 & -2A_4A_2 & -2A_4A_3 & 1 - 2A_4^2 & 2A_4A_5 \\ -2A_5A_1 & -2A_5A_2 & -2A_5A_3 & -2A_5A_4 & 1 + 2A_5^2 \end{pmatrix} \begin{pmatrix} a_1 \\ a_2 \\ a_3 \\ a_4 \\ a_5 \end{pmatrix}$$

Note that the components of the inversion matrix depend only on the inversion coordinates of the inversion sphere. Therefore, for an inversion sphere it is enough to calculate the corresponding inversion matrix once. This reduces dramatically the computation time.

Bibliography

[1] A. Drescher and G. de Josselin de Jong. *J. Mech. Phys. Solids*, 20:337, 1972.

[2] S.S. Manna and H.J. Herrmann. *Eur. Phys. J. E*, 1:341–344, 2000.

[3] P. Richard. *Nature Materials*, 4:121128, 2005. doi:10.1038/nmat1300.

[4] S.B. Savage and C.K.K. Lun. *J. Fluid Mech.*, 189:311, 1988.

[5] G.C. Barker. In *Granular Matter*, page 35, Heidelberg, 1994. Springer.

[6] H.J. Herrmann. In *Third Granada Lectures in Computational Physics*, page 67, Heidelberg, 1995. Springer.

[7] S.R. Nagel H.M. Jaeger and R.P. Behringer. *Rev. Mod. Phys.*, 68:1259, 1996.

[8] J. Duran. *Sands, Powders, and Grains: An Introduction to the Physics of Granular Materials*. Springer-Verlag, New York., 2000.

[9] M. Rodhes. *Principles of powder technology*. John Wiley & Sons, 1997. ISBN 0-471-92422-9.

[10] M.E. Fayed and L. Otten. *Handbood of powder science & technology*. Springer, 1997. Second edition.

[11] S. Fauve S. Douady and C. Laroche. *Europhys. Lett.*, 8:621, 1989.

[12] T. Pöschel J.A.C. Gallas, H.J. Herrmann and Sokolowski. *J. Stat. Phys.*, 82:443, 1996.

[13] J. Rajchenbach S. Luding, E. Clément and J. Duran. *Europhys. Lett.*, 36:247, 1996.

[14] J.B. Swift W.D. McCormick C. Bizon, M.D. Shattuck and H.L. Swinney. *Phys. Rev. Lett.*, 80:57, 1998.

[15] F. Prinz A.D. Rosato, K.J. Strandburg and R. H. Swendsen. *Phys. Rev. Lett.*, 249:1038, 1987.

[16] O.R. Walton. page 327, Amesterdam, 1983. Elsevier.

[17] D. Hirchfeld and D.C. Rapaport. *Phys. Rev. E.*, 56:2012, 1997.

[18] M. Faraday. *Philos. Trans. R. Soc. London*, 52:299, 1831.

[19] J. Rajchenbach E. Clément, L. Vanel and J. Duran. *Phys. Rev. E*, 53:2972, 1996.

[20] S. Douady C. Laroche and S. Fauve. *J. Phys. (Paris)*, 50:699, 1989.

[21] E. Clément J. Duran, T. Mazozi and J. Rajchenbach. *Phys. Rev. E*, 50:3092, 1994.

[22] P. K. Haff. *J. Fluid Mech.*, 134:401, 1983.

[23] H. K. Pak and P. P. Behringer. *Phys. Rev. Lett.*, 71:1832, 1993.

[24] P. Umbanhowar F. Melo and H. L. Swinney. *Phys. Rev. Lett.*, 72:172, 1994.

[25] J. T. Jenkins and S. B. Savage. *J. Fluid Mech.*, 130:187, 1983.

[26] F. de Larrard. *Concrete mixture proportioning*. Eds. E & FN Spon. London, New York, 1999.

[27] K. Iwashita M. Oda and H. Kazama. In *Proceedings of the IUTAM Symposium on Mechanics and Porous Materials*, pages 353–364, Kluwer, The Netherlands, 1997.

[28] J.P. Bardet. *Mech. Matter*, 18:159, 1994.

[29] H.J. Herrmann J.A. Åström and J. Timonen. *Phys. Rev. Lett.*, 84:638, 2000.

[30] Tomaso Aste and Denis Weaire. *The pursuit of perfect packing*. Nicki Dennis, London, 2000.

[31] F. Soddy. *Nature*, 137:1021, 1936.

[32] G. Mantica H.J. Herrmann and D. Bessis. *Phys. Rev. Lett.*, 65:3223–6, 1990.

[33] G. Oron and H. J. Herrmann. *J. Phys. A:Math. Gen.*, 33:1417–1434, 2000.

[34] D. Bideau and A. Hansen. *Disorder and granular media*. North-Holand, Amsterdam, 1993.

[35] D.J. Cumberland and R.J.Crawford. *The packings of particles*. Elsevier, Amsterdam, 1987.

[36] F. Alonso-Marroquin and H.J. Herrmann. *Phys. Rev. Lett.*, 92:054301, 2004.

[37] F. Alonso-Marroquin and H.J. Herrmann. *Phys. Rev. E*, 66:021301, 2002.

[38] S.S. Manna. *Physica A*, 187(3-4):373, 1992.

[39] N.V. Brilliantov Y.A. Andrienko and P.L. Krapivsky. *J. Stat. Phys.*, 75(3-4):507, 1994.

[40] P.L. Krapivsky N.V. Brilliantov and Y.A. Andrienko. *J. Phys. A.:Math. Gen.*, 27:L381, 1994.

[41] P.S. Dodds and J.S. Weitz. *Phys. Rev. E*, 56:056108, 2002.

[42] H.S. Horn. *The adaptive geometry of trees*. Princeton University Press, 1971.

[43] K. Takahashi. *Annals of Botany*, 77:159, 1996.

[44] S.C. van der Marck. *Phys. Rev. Lett.*, 77:1785, 1995.

[45] D. Turcotte. *Fractals and chaos in geology and geophysics*. Cambridge University Press, 1997. 2d ed.

[46] C. Hecht. *Pure Appl. Geophys.*, 157:487, 2000.

[47] N. Sloane J. Conway. *Sphere packings, lattices and groups*. Springer-Verlag, New York, 1999. 3rd. ed.

[48] H.J. Herrmann S. Roux, A. Hansen and J.-P. Vilotte. *Geophysical Research Letters*, 20:1499–1502, 1993.

[49] C. Lomnitz. *Bull. Seismol. Soc. Am.*, 72:1441, 1982.

[50] L. Sykes W. McCann, S. Nishenko and J. Krause. *Pure Appl. Geophys.*, 117:1082, 1979.

[51] C.C. Barton. In *C.C. Barton, P.R. LaPointe (Eds.)*, page 141, New York, 1995.

[52] R. Biegel C. Sammis, G. King. *Pure Appl. Geophys.*, 125:777, 1987.

[53] K.P. Kodama. *J. Geophys. Res.*, 93:3357–3371, 1988.

[54] T. Aifa J.P. Pozzi. *Phys. Earth Planet. Int.*, 58:255–266, 1989.

[55] A. Grisard. In *Projet de 3e Année, PMMH, ESPCI*, Paris, 1991.

[56] H.J. Herrmann J.A. Åström and J. Timonen. *Phys. Rev. Lett.*, 84:638–641, 2001.

[57] R. Mahmoodi Baram H.J. Herrmann, J.A. Åström. *Physica A*, 344:316–522, 2004.

[58] D. C. Rapaport. *The art of molecular dynamics simulation*. Cambridge University Press, Cambridge, 1995.

[59] M. P. Allen and D. J. Tildesley. *Computer simulation of liquids*. Oxford University Press, 1989.

[60] J. A. McCammon and S. C. Harvey. *Dynamics of proteins and nucleic acids*. Cambridge University Press, 1987.

[61] D. Frenkel and B. Smit. *Understanding molecular simulation*. Academic Press, 2001.

[62] J.M. Haile. *Molecular Dynamics Simulation: Elementary Methods*. 2001.

[63] B. Roux O.M. Becker, Alexander D. Mackerell Jr and M. Watanabe. *Computational biochemistry and biophysics*. Marcel Dekker, 2001.

[64] T. Schlick. *Molecular Modeling and Simulation*. Springer, 2002.

[65] M. Jean and J.J. Moreau. In *Proceedings of Contact Mechanics International Symposium*, pages 31–48, Lausanne, Switzerland, 1992. Presses Polytechniques et Universitaires Romandes.

[66] J.J. Moreau. *Eur. J. Mech. A-Solids*, 13:93–114, 1994.

[67] S. Roux F. Radjai and J. Moreau. *Chaos*, 9:544–550, 1999.

[68] D.E. Wolf. In *Computational Phyics*, Berlin, 1996. Springer.

[69] S. McNamara and W.R. Young. *Phys. Rev. E*, 50:R28–R31, 1994.

[70] D.W. Boyd. *Can. J. Math.*, 25(2):303–322, 1973.

[71] D.W. Boyd. *Mathematika*, 20:170–174, 1973.

[72] D.W. Boyd. *Math. Comp.*, 39(159):249–254, 1982.

[73] S.S. Manna and H.J. Herrmann. *J. Phys. A: Math. Gen.*, 24:L481–L490, 1991.

[74] and R. Peikert M. Borkovec, W. de Paris. *Fractals*, 2(4):521–526, 1994.

[75] B. B. Mandelbrot. *The fractal geometry of nature*. Freeman, San Francisco, 1982.

[76] and D. Wright D. Mumford, C. Series. *Indra's pearls*. Cambridge University Press, Cambridge, 2002.

[77] N. Rivier. *Phil. Mag. A*, 40:859–868, 1979.

[78] R. Mahmoodi Baram and H.J. Herrmann. *Fractals*, 12:293–301, 2004.

[79] H.J. Herrmann R. Mahmoodi Baram and M. Wackenhut. *Physica A*, 330:77–82, 2003.

[80] H.J. Herrmann R. Mahmoodi Baram and M. Wackenhut. *Physica A*, 33:591, 2003.

[81] R. Mahmoodi Baram M. Wackenhut and H.J. Herrmann. to be published in J. of Phys. CM.

[82] R. Mahmoodi Baram M. Wackenhut and H.J. Herrmann. In *hmoodi Baram, M. Wackenhut, and H.J. Herrmann,* The art of packing densely. *Proceedings of the International Conference on Statistical Physics of Complex Fluids*, Zanjan, Iran, 2004. to be published in J. of Phys. CM.

[83] R. Mahmoodi Baram H.J. Herrmann and N. Rivier. *Phys. Rev. Lett.*, 92:044301, 2004.

Acknowledgment

I thank all those who made this work possible.

I wish to express my sincere gratitude to Prof. Dr. Hans J. Herrmann who gave me this unique opportunity to work at ICA1, and offered me an excellent guidance and a continuous encouragement throughout this work.

I also thank those people who contributed in some way to this work, especially to Martin Strauß, Martin Wackenhut, Sean McNamara, Jens Harting, Frank Raischel and Hans-Joerg Seybold for their useful comments and translating the abstract of my thesis into german.

I am also grateful to the members of the ICA1, Stuttgart, who indirectly supported this work by an excellent working atmosphere. I also thank our very kind secretary Marlies Parsons who helped me to survive in Germany, and Frank Huber for solving problems related with the computers.

Reza Mahmoodi Baram
July 4, 2005
Stuttgart, Germany